Palynological and geochemical assessment of the Late Triassic in the high-latitude section of Festningen (Svalbard)

Name: Floris Vink Student number: 7680805 E-mail: f.h.f.vink@students.uu.nl

MSc thesis ECTS: 45 Final version: 7-7-2024

First supervisor: Bas van de Schootbrugge, Universiteit Utrecht, b.vanderschootbrugge@uu.nl

Second supervisor: Remco Bos, Universiteit Utrecht, r.bos@uu.nl

Abstract

The Late Triassic (237-201.4 Ma) is characterized by several biotic turnovers and carbon isotope perturbations, commonly linked to large-scale volcanism. In order to examine the extent of volcanic-induced kill mechanisms, records from high-latitude sites are required to assess the global impact on the biosphere, as most data has been recorded in mid-latitude sites in NW Europe. To this end, the floral turnovers and geochemical perturbations of an Upper Triassic succession are examined from a high-latitude section at Festningen (Svalbard). The Festningen section contains vertical sedimentary outcrops continually exposing from the Upper Carboniferous to Palaeogene. Contradicting biostratigraphic age interpretations have been put forth in studies on the Upper Triassic Knorringfjellet Formation (Wilhelmøya Subgroup). Here, palynological and geochemical (carbon) examinations are presented which identify floral trends and carbon cycle perturbations that indicate environmental disturbances. A new stratigraphic framework is constructed based on palynomorph content. In addition, thin sections of phosphate rich beds were investigated from the lower Knorringfjellet Formation.

The dinoflagellate cyst dominated lower interval of the Knorringfjellet Formation is of a Norian age and seems to reflect an Arctic circumpolar correlative event. In the upper interval of the Knorringfjellet Formation the apparent occurrence of the Jurassic marker species *Cerebropollenites thiergartii* (recently recombined as *Sciadopityspollenites thiergartii*) together with abundant Triassic marker species results in divergent age interpretations. Here, a Rhaetian age is proposed for this interval, as *C. thiergartii* is occasionally reported in the Rhaetian and its first occurrences vary between localities. The results cast further doubt on the reliability of *C. thiergartii* as a marker for the base of the Jurassic. Similar reports of *C. thiergartii* in Triassic assemblages in northern Norway might indicate the taxa originated in high-latitude regions.

Phosphatic coated grains identified in the Norian phosphate rich beds indicate disturbed anoxic conditions, possibly linked to intensified oceanic upwelling resulting from climate warming. This bed could be correlated to temperature peaks around the Carnian-Norian boundary or to the mid-late Norian Angayucham LIP, as dating is not very precise. Vegetational reconstruction reveals a mire landscape dominated by ferns and cycads/ginkgos, with conifers prevailing in drier areas. In the lower Rhaetian interval an increase in xerophytic taxa might indicate a period of relatively drier conditions. No spore spikes indicating environmental disturbance were found. A decrease in dinocysts coinciding with a foraminiferal discontinuity indicates a marine turnover during the Rhaetian. A CIE possibly correlated to the precursor CIE, or an earlier Rhaetian carbon cycle perturbation, is recognized at the top of the interval analysed in this study.

1. Introduction

The Late Triassic is characterized by several carbon isotope perturbations, commonly linked to large-scale volcanism and biotic turnovers. The end-Triassic mass-extinction event (ETME), linked to Central Atlantic Magmatic Province (CAMP) volcanism (Wignall, 2001), is considered one of the largest biotic crises of the Phanerozoic (McGhee et al., 2013). In Europe, main pulses of floral turnover in the end-Triassic coincide with negative excursions in $\delta^{13}C$ records, indicating the phases of CAMP activity strongly impacted terrestrial vegetation (Bos et al., 2023; Lindström, 2021; Wignall & Atkinson, 2020). The floral turnover is characterized by a decline in pollen producing arborescent conifers, followed by a spike in spore producing ferns and fern allies (Bos et al., 2023; Lindström, 2021), a typical pattern for a period of environmental disturbance. The extinction interval culminated with the extinction of Triassic vegetation and dinocyst taxa at the Triassic-Jurassic boundary (Bos et al., 2023; Van de Schootbrugge et al., 2013). Earlier phases of volcanism linked to carbon isotope perturbations and global warming have been reported during the late Norian and in the mid-Carnian. A late Norian global warming interval aligns with carbon isotopic perturbations and the approximate dating of the volcanic deposits of the Angayucham Large Igneous Province (LIP) (Sato et al., 2023). The Wrangellia Terrane LIP coincides with negative $\delta^{13}C$ shifts during the Carnian Pluvial Episode (CPE) (Dal Corso et al., 2018).

The majority of the research on this time period has been performed in Europe, where the stratigraphy is relatively well-defined after years of research. Outside of Europe the extent of floral turnover and possible impact of volcanism during the Late Triassic is poorly studied. To better understand the global mechanisms in the Late Triassic data from higher latitudes are needed. Analysis of the Festningen section in Svalbard allows us to get data from a high northern paleolatitude, which can then be compared to the mid-latitude European sites.

The Festningen area is a classical section in western central Spitsbergen studied since the 1930´s (Frebold, 1930; Hoel & Orvin, 1937). The Festningen section contains the thickest and most complete succession in Svalbard (Vigran et al., 2014), continually exposing deposits from the Upper Carboniferous to the early Cenozoic (Hoel & Orvin, 1937; Winsnes et al., 1962). Upper Triassic and Lower Jurassic deposits in western central Spitsbergen are represented by the Knorringfjellet Formation from the Wilhelmøya Subgroup, which is developed stratigraphially condensed (Mørk et al., 1999; Nagy & Berge, 2008; Vigran et al., 2014). The palynology of the Festningen section was earlier analysed semi-quantitatively in a large scale study by Vigran et al. (2014), this study will focus on the Knorringfjellet Formation at Festningen in a higher detail.

Vigran et al. (2014) and Rismyhr et al. (2018) have published contradicting biostratigraphic age interpretations for the Knorringfjellet Formation at Festningen. Vigran et al. (2014) propose a transition to the Jurassic occurs in the middle of the formation based on the occurrence of the Jurassic marker species *Cerebropollenites thiergartii* (recently recombined as *Sciadopityspollenites thiergartii*). Rismyhr et al. (2018) argue against this interpretation and propose the complete Knorringfjellet Formation at Festningen consists of Norian deposits. This is based on the dominating presence of typical Late Triassic palynomorphs and the absence of any other taxa characteristic of the Early Jurassic throughout the upper part of the formation.

Here, the extent of floral turnover and the possible impact of volcanism are studied by reconstructing vegetational history and identifying possible environmental disturbances in the Upper Triassic Festningen section in Svalbard. The ages of the sediments of the Knorringfjellet Formation are investigated and a new biostratigraphic age interpretation is proposed based on the occurrences of Triassic and Jurassic palynological marker species. A vegetational reconstruction is made based on relative abundances of different floral groups and shifts in the abundances of aquatic dinoflagellate cysts and acritarchs are revealed. It is tested if a decrease in conifer pollen and spike in fern spores

similar to Europe can be identified. Samples are also analysed for organic $\delta^{13}C$ and Total Organic Carbon (TOC) to find perturbations in the carbon cycle, which are compared to earlier reported carbon isotope excursions (CIEs).

The phosphate rich Slottet Bed covers the lower 3 m of the Knorringfjellet Formation. Late Rhaetian phosphate rich beds from Europe and Canada have been theorized to indicate disturbed anoxic/euxinic environments, possibly related to volcanic induced climate warming (Suan et al., 2012; Larina et al., 2019). Petrographic thin sections from the Slottet Bed are therefore investigated for phosphatic coated grains, which might be similar in shape and origin to the coated grains reported by Larina et al. (2019). The uppermost interval of the Knorringfjellet Formation was covered in snow during sample collection, consequently this study is restricted to the lower 10 m of the formation.

2. Background

2.1 Environmental change during the Late Triassic

The Late Triassic epoch consists of the Carnian, Norian and Rhaetian stages. Throughout the Late Triassic several periods of large-scale volcanism, global warming, biotic turnover and carbon cycle perturbations have been reported.

During the Carnian large volumes of flood basalts erupted to form the Wrangellia Terrane LIP in western North America. Multiple negative $\delta^{13}C$ shifts are recorded in the mid-Carnian (figure 1), at the onset of the Carnian Pluvial Episode (CPE) (Dal Corso et al., 2018), an interval of major climatic and biotic change with more humid conditions. This series of carbon cycle perturbations is likely caused by the release of light carbon during multiple high-intensity pulses of Wrangellia LIP volcanism (Dal Corso et al., 2018; Dal Corso et al., 2012), which may have played a major role in driving biotic and climatic changes during the CPE (Jin et al., 2023). Following the CPE, an intense warming period occurred during the mid-late Carnian (figure 1; Trotter et al., 2015). A turnover among terrestrial vertebrates and plants is found at the Carnian-Norian boundary, which might be explained by a return to arid conditions, after increased rainfall during the CPE (Simms & Ruffell, 1989).

A long period of sustained cooler conditions is found during much of the Norian (Trotter et al., 2015). A warming trend reinstated towards the late Norian, reaching a humid hothouse climate comparable to the PETM by the middle-late Norian (Sun et al., 2020; Trotter et al., 2015). This interval of strongly increased sea surface temperatures aligns with carbon isotopic perturbations and the approximate dating of the volcanic deposits of the Angayucham LIP (figure 1; Sato et al., 2023). Multiple negative $\delta^{13}C_{org}$ shifts have been identified during the late Norian; this interval has been called the Norian “chaotic carbon episode” (Sato et al., 2023; Zaffani et al., 2017). The Angayucham Terrane is a LIP dated to the Norian, cropping out in Alaska (figure 2), with an estimated age of 214 ± 7 Ma (Ernst & Buchan, 2001; Prokoph et al., 2013). The total volume of the Angayucham LIP is estimated at 225.000-450.000 km^3, based on an evaluation from areal extent of outcrops (Ernst and Buchan, 2001; Prokoph et al., 2013). Osmium isotope data reveal two negative shifts in the $^{187}Os/^{188}Os$ ratio during a negative CIE in the lower Sevatian (lower upper Norian), which are suggested to be caused by the onset of the Angayucham volcanism (Sato et al., 2023).

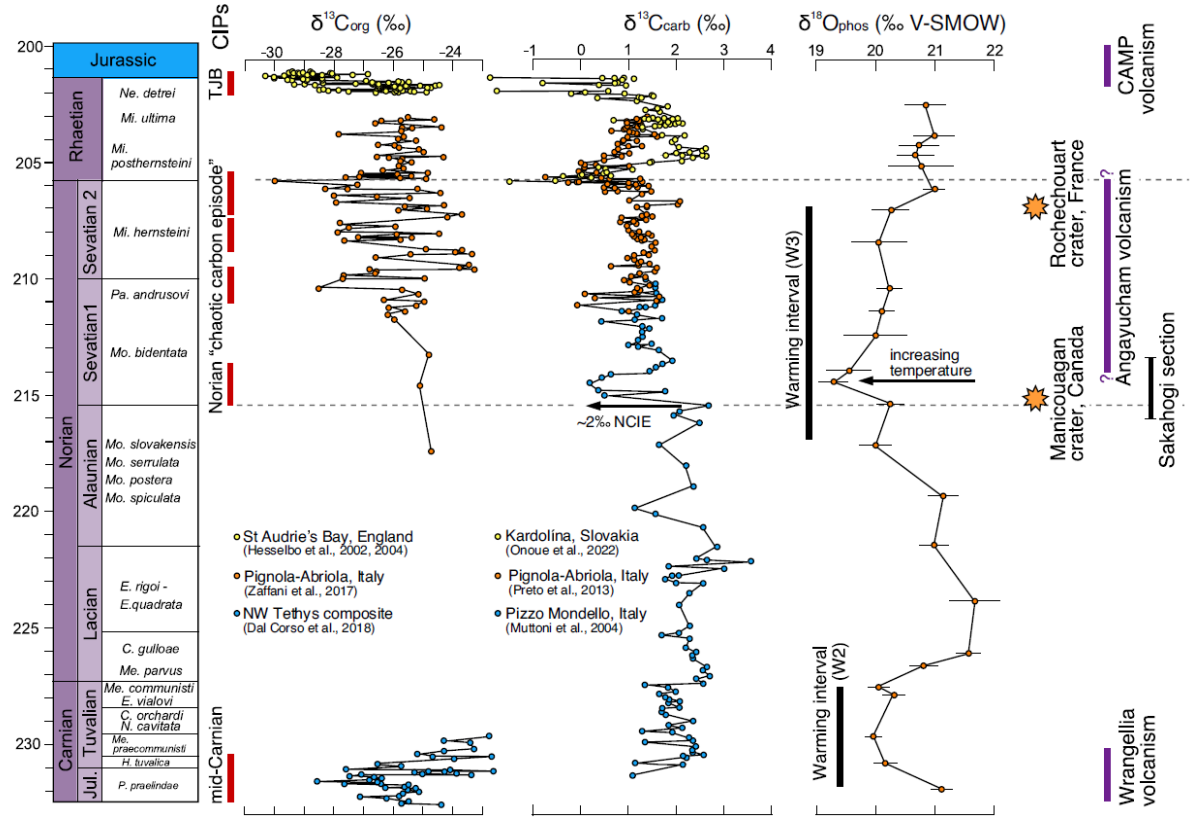

Figure 1: Overview of Late Triassic $\delta^{13}C$ records and oxygen isotope records ($\delta^{18}O_{phos}$; from Trotter et al., 2015). Major carbon isotope perturbation episodes (CIPs) are present in the mid-Carnian, the late Norian, and around the Triassic-Jurassic boundary (TJB). W2 and W3 are the two major warming intervals in the Late Triassic. The three large igneous provinces from the Late Triassic are indicated on the right (Wrangellia, Angayucham, and Central Atlantic Magmatic Province: CAMP) (Sato et al., 2023).

Rigo et al. (2020) suggest the onset of Late Triassic extinctions is found at or around the Norian-Rhaetian boundary. The start of declining diversity at this boundary coincides with a carbon perturbation, indicating that climatic and environmental changes might have impacted the biota at a global scale. Clement et al. (2024) hypothesize increased hydrothermal venting or subaqueous basalt emplacement could explain the unique fingerprint of the Norian-Rhaetian boundary. After the late Norian warming interval, much of the Rhaetian was characterized by decreased sea surface temperatures (figure 1; Trotter et al., 2015). Mid-Rhaetian microfossil assemblages from Nevada, USA, show evidence for intermitted oxygen depletion, indicating environmental stress occurred during much of the Rhaetian and not exclusively during the latest Rhaetian (Clement et al., 2024).

The late Rhaetian volcanic activity of the Central Atlantic Magmatic Province (CAMP; figure 2), during the breakup of Pangea, has been shown to be synchronous with the ETME (Blackburn et al., 2013; Dal Corso et al., 2014; Hesselbo et al., 2002; Whiteside et al., 2010; Wignall, 2001), and is therefore generally held responsible for this major crisis. Large amounts of isotopically light carbon released by volcanism resulted in negative isotope excursions in organic $\delta^{13}C$ records and increased atmospheric pCO_2 (Ruhl et al., 2011). This rise in atmospheric pCO_2, and the global warming associated with this, are thought to be the main trigger of environmental disturbance during the ETME (Hesselbo et al., 2002; Ruhl et al., 2011).

The first disruption of the carbon cycle at the end of the Rhaetian is identified as the precursor/Marshi Carbon Isotope excursion (CIE) (Ruhl & Kürschner, 2011) and is related to the earliest CAMP mafic intrusions (Davies et al., 2017). Around this carbon perturbation phosphate rich beds from before the extinction interval have been described, possibly related to volcanic induced climate warming (Suan et al., 2012; Larina et al., 2019). A sharp and high amplitude negative CIE has been detected at the latest Rhaetian, the Initial/Spelae CIE, approximately coinciding with the Triassic-Jurassic boundary. This is followed in the earliest Triassic by the main/Tilmanni CIE, which is of lower amplitude but longer duration (Hesselbo et al., 2002).

The ETME coincides with major shifts in vegetation (Van de Schootbrugge et al., 2009). Research across Europe has shown there was a two phased pattern of extinction in terrestrial as well as marine organisms (Bos et al., 2023; Lindström, 2021; Wignall & Atkinson, 2020). These two main pulses of increased extinction rates coincide with negative excursions in $\delta^{13}C$ records, indicating the phases of CAMP activity strongly impacted terrestrial vegetation and marine biota (Lindström et al., 2021; Wignall & Atkinson, 2020). The first floral turnover occurred after the precursor CIE and is characterized by a decline in arborescent conifers (Bos et al., 2023; Lindström, 2021). Following this decline, a stepwise rise of ferns and fern allies is found at the cost of trees during the latest Rhaetian (Bos et al., 2023). The first extinction phase coincides with a regression (Wignall & Atkinson, 2020). The second phase of increased extinction rates is correlated with the initial CIE (Lindström, 2021). This phase culminated with the extinction of Triassic taxa at the Triassic Jurassic boundary (Bos et al., 2023) and resulted in a major shift in the dominant floral biomes, establishing Early Jurassic vegetation (Lindström, 2016). The second extinction phase occurs at a flooding surface, marked by the spread of anoxia (Wignall & Atkinson, 2020). In the marine realm most Triassic dinoflagellate cysts dissapear in the extinction interval, being replaced by acritarchs and prasinophytes seen as ‘disaster taxa’ (van de Schootbrugge et al., 2007).

2.2 Geological setting

The Svalbard archipelago is part of the Eurasian continental plate and is located on the northwestern margins of the present-day Barents Shelf. This part of the Barents Shelf has been uplifted, exhumed and folded (Worsley, 2008). The Barents Shelf is an intracratonic basin, bounded by passive margins developed in the Cenozoic on its western and northern flanks (Faleide et al., 2015). The Barents shelf was part of a large epicontinental sea during the Mesozoic (figure 2); it was surrounded by Pangaea with one open connection towards the Boreal part of the Panthalassa Ocean in the northwest (Riis et al., 2008).

Throughout most of the Triassic the region was characterized by sag basin subsidence and a thick siliciclastic succession recording delta progradation was deposited (Riis et al., 2008). In Svalbard, a shift in the source of the sediment input occurred in the Late Triassic. During the Early and Middle Triassic westerly sediment input from North Greenland has been recorded, which was replaced during the Late Triassic as dominant Uralian-sourced systems from the southeast and east reached Svalbard (Bue & Andresen, 2013). Supplied by sediments sourced from the Uralides, a large prograding delta system formed in the Barents Sea basin (De Geerdalen Formation, see chapter 2.3). This prograding delta system formed an extensive low-gradient delta plain that covered most of the Barents Shelf by the end of the Carnian (Høy & Lundschien, 2011; Riis et al., 2008).

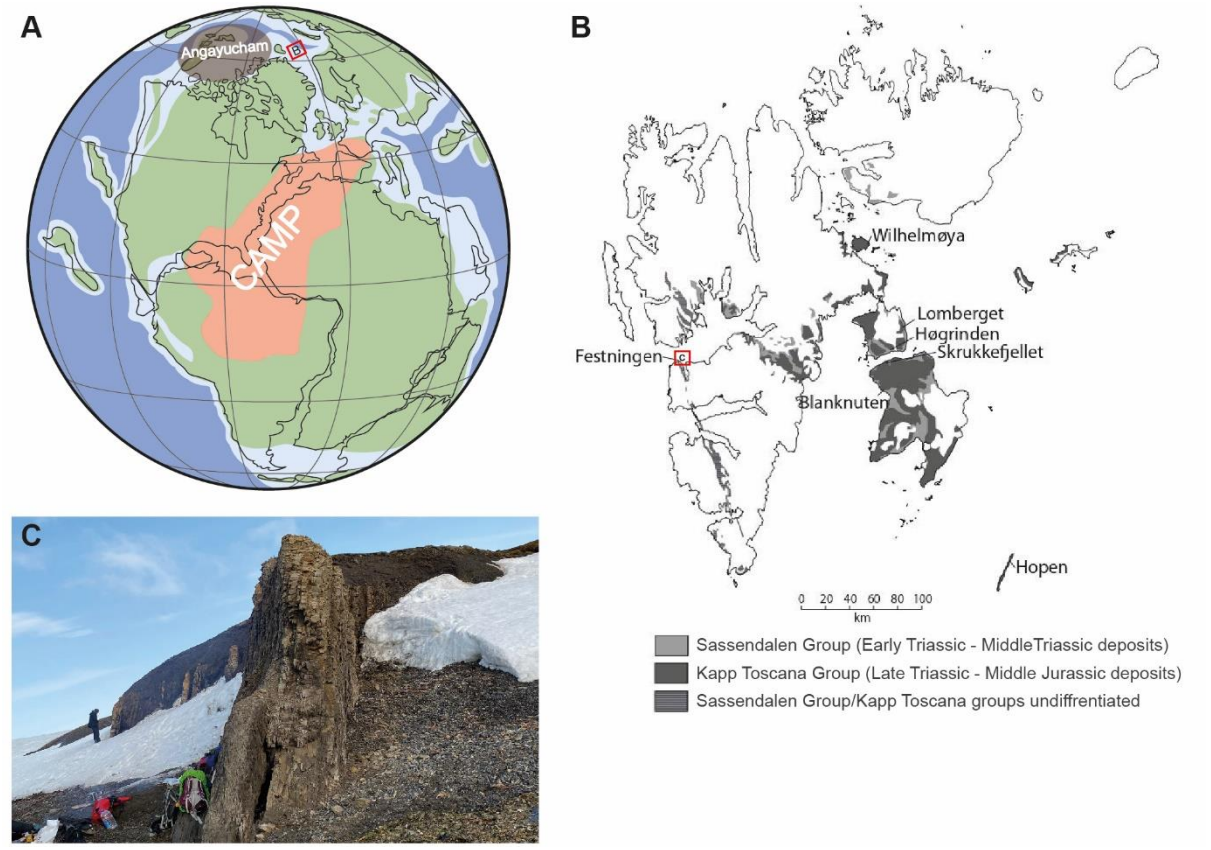

Figure 2: Paleogeography and modern location of the study area. A. Global reconstruction of the continental configuration and position of the Panthalassa and Tethys Oceans in the Late Triassic (modified after Bos et al. 2023) with the location of Svalbard marked by a red rectangle. The areas of the Central Atlantic Magmatic Province (~201 Ma, after Bos et al., 2023) and the Angayucham LIP (214 ± 7 Ma, after Sato et al., 2023) are indicated. B. Map of modern day Svalbard showing the location of commonly studied localities and Triassic to mid-Jurassic exposures (Vigran et al., 2014), the Festningen locality in western central Spitsbergen is marked by a red rectangle. C. A photo of the Upper Triassic succession of the Festningen section, from which the samples of this study were taken.

An early Norian transgression was accompanied by changes in dominant provenance areas and a decrease in subsidence rate in the latest Triassic-Early Jurassic (Bergan & Knarud, 1993; Fleming et al., 2016; Ryseth, 2014). This might have been the result of forebulge development in the central Barents shelf area, as well as uplift and possible rejuvenation of more proximal areas and basin margins (Rismyhr et al., 2018). The Barents Sea basin experienced mild inversion in the Late Triassic-Early Jurassic, because the Siberian plate margin was pushed into Novaya Zemlya (Buiter & Torsvik, 2007). A slower rate of subsidence in the latest Triassic-Early Jurassic led to repeated resedimentation and both textural and mineralogical maturation (Bergan & Knarud, 1993). The Upper Triassic-Middle Jurassic succession in Svalbard records shallow marine to coastal sediments and becomes more stratigraphically condensed towards the basin margins and over regional platforms and highs, characterized by internal disconformities. This indicates there were large lateral variations in accommodation space (Rismyhr et al., 2018). Zircon age data of Late Triassic-Early Jurassic sands in Svalbard suggest Triassic sediments were mixed in, indicating reworking of older strata and possible renewed input of sediments from the west (Bue & Andresen, 2013).

The late Middle Jurassic marks the onset of rifting in the western Barents Shelf (Faleide et al., 2015). During Early Cretaceous time the Bjornoya, Tromso and Harstad Basins developed as prominent rift basins in the south-western Barents Shelf, following regional extension accompanied by strike-slip adjustments (Faleide et al., 2015; Faleide et al., 1993). Several later phases of rifting in the Late Mesozoic and Early Cenozoic gave rise to very deep basins in the southwestern Barents Shelf (Faleide et al., 2015). In the late Palaeocene to Eocene the West Spitsbergen Fold-and-Thrust Belt was developed (Steel et al., 1985), which had a significant impact on the orientation of the strata at Festningen. During the latest Palaeogene-Quaternary the area was uplifted and (largely glacial) erosion took place (Dimakis et al., 1998). These tectonic events and the recent erosional phase led to a clear exposure of the Festningen succession at sea level, with strata dipping steeply eastwards (Rismyhr et al., 2018).

2.3 Stratigraphy of the study area

The Upper Triassic to Middle Jurassic succession of Svalbard is grouped in the Kapp Toscana Group, which attains a total thickness of 300– 350 m in western central Spitsbergen. The group encompasses the Tschermakfjellet Formation (early Carnian), the De Geerdalen Formation (Carnian-early Norian) and the Knorringfjellet Formation of the Wilhelmøya Subgroup (early Norian-Bathonian) (Rismyhr et al., 2018; Vigran et al., 2014). The Kapp Toscana Group is topped by offshore mudstones and siltstones of the 500 m thick Agardhfjellet Formation (Middle Jurassic to Lower Cretaceous) from the Adventdalen Group (Koevoets et al., 2018).

The De Geerdalen Formation comprises the largest part of the Kapp Toscana Group, with a thickness of nearly 300 m. In this member repeated coarsening-upward successions from shales to sandstones (Mørk et al., 1999) reflect a prograding delta system, mainly from the southeast (Klausen et al., 2015; Rød et al., 2014). Mudstones alternating with thin siltstones and sandstones of the Isfjorden Member form the uppermost 70 m of the De Geerdalen Formation (Mørk et al., 1999). This member records deposition in shallow shelf, lagoonal and delta-plain environments (Lord et al., 2017; Rød et al., 2014).

Upper Triassic and Lower Jurassic deposits in western central Spitsbergen are represented by the Knorringfjellet Formation from the Wilhelmøya Subgroup, which disconformably overlies the De Geerdalen Formation (Mørk et al., 1999; Nagy & Berge, 2008; Vigran et al., 2014). The Knorringfjellet Formation forms the Wilhelmøya Subgroup together with time equivalent formations elsewhere in Svalbard. Despite the disconformable nature of the De Geerdalen Formation-Wilhelmøya Subgroup boundary, no major hiatus has been documented so far based on biostratigraphic data (Paterson & Mangerud, 2015; Vigran et al., 2014).

The Knorringfjellet Formation at Festningen is developed at a thickness of 17.5 m (Bäckström & Nagy, 1985). The base of this formation is characterized by a ~20 cm thick polymict conglomerate bed dominated by phosphate nodules, overlain by medium-grained highly bioturbated sandstones. This bed, covering the lower 3 m of the member, is called the Slottet Bed (Mørk et al., 1999; Nagy & Berge, 2008; Vigran et al., 2014). The stratigraphic position of the Slottet Bed suggests the conglomerate was accumulated mainly as lags formed by wave reworking and winnowing of underlying substrates during relative sea-level rise (Rismyhr et al., 2018). The sedimentology of the lower part of the formation shows a fining-upwards transgressive development (Rismyhr et al., 2018) and foraminiferal tests found in thin sections of the basal conglomerate are in accordance with this marine transgressive nature (Nagy & Berge, 2008). The phosphatic conglomerate at the base of the Slottet Bed grades upward into shoreface sandstones and is subsequently overlain by offshore shales and a layer with glauconitic deposits. This sequence suggests upward-deepening and potentially an upwards decrease in sedimentation rates (Rismyhr et al., 2018). The precipitation of

the authigenic glauconite is characteristic for a condensed section deposited at a time of maximum transgression of the shoreline (Loutit et al., 1988). Therefore, Rismyhr et al. (2018) place a maximum flooding surface (MFS) at this glauconitic deposit, marking a transition from a transgression to a regression.

The overlying succession consists of an alternation of deeper marine shale intervals and siderite cemented sandstone beds, which are suggested to be shoreface water depth deposits (Nagy & Berge, 2008; Vigran et al., 2014). The shale intervals were deposited below the fair-weather wave base or even below the storm wave base (Nagy & Berge, 2008). The sandstones are densely cemented and heavily bioturbated, and most primary sedimentary structures have been destroyed due to this biogenic mixing. Diffuse lamination in the shales suggests a low degree of bioturbation in these intervals (Nagy & Berge, 2008). The marine character of the formation is affirmed by its saurian bone content and marine type trace fossils (Bäckström & Nagy, 1985). The complete succession is interpreted as a transgressive-regressive sequence with a more condensed nature at the top and no or only limited preservation of its regressive portion (Rismyhr et al., 2018). The top of the formation is marked by another conglomerate bed with phosphate nodules; the Brentskardhaugen Bed (Mørk et al., 1999; Vigran et al., 2014). The contact between this Brentskardhaugen Bed and the Knorringfjellet Formation is erosional (Bäckström & Nagy, 1985).

The Knorringfjellet Formation comprises two informally named subunits: the Tverrbekken and Teistberget Members (Mørk et al., 1999). The subdivision is made based on the placement of a major hiatus between the two members; with the lower Tverrbekken Member constituting the Upper Triassic interval of the formation and the overlying Teistberget Member comprising its Lower Jurassic part (Korčinskaja, 1980; Mørk et al., 1999). This subdivision is not used by Rismyhr et al. (2018), who prefer a subdivision in three sequences separated by disconformities.

The Knorringfjellet Formation contains diverse palynological assemblages; dinoflagellate cysts and spores are more abundant than pollen (Vigran et al., 2014). The cyst assemblage shows similarities with the marine horizon from Arctic Canada described by Bujak and Fisher (1976), which may reflect a circumpolar correlative event (Vigran et al., 2014). The foraminiferal succession of the Knorringfjellet Formation consists mostly of agglutinated taxa, with extremely low assemblage diversities and a dominance of small-sized species (Nagy & Berge, 2008). This micropaleontological evidence indicates restricted environmental conditions, mostly caused by hyposaline environments and, to a lesser extent, hypoxia in near-bottom waters. The extremely low calcium carbonate content of the shales in the formation is in accordance with hyposaline conditions. These conditions were likely caused by high freshwater input creating density stratified water masses (Nagy & Berge, 2008).

The Wilhelmøya Subgroup in western central Spitsbergen is developed relatively thin, with a thickness around 15-20 m, and contains several closely spaced hiatuses (Vigran et al., 2014). This stratigraphic condensed development is interpreted to be the result of very low subsidence rates and thus limited accommodation space and low sedimentation rates during the Late Triassic-Middle Jurassic interval in Spitsbergen (Johannessen & Embry, 1989; Rismyhr et al., 2018). The epicontinental setting of the Barents Shelf during the Late Triassic to Middle Jurassic points towards a basin physiography with a very gentle depositional gradient. This is supported by the relatively small variations in total thickness of the Wilhelmøya Subgroup in western central Spitsbergen (Rismyhr et al., 2018). A low gradient shelf like this is highly sensitive to relative sea-level fluctuations, and even modest sea level changes may cause rapid and significant relocations of the shoreline (Posarnentier & Allen, 1999). A rise in relative sea level would lead to rapid landward migration of the shoreline, trapping sediments within the coastal zone. As a result, more distal parts of the shelf would become starved of clastic sediment and thereby more susceptible for the precipitation of authigenic minerals; for example the phosphate found in the Wilhelmøya Subgroup (Rismyhr et al., 2018). A fall in relative sea level in this type of low gradient shelf would allow river systems to rapidly extend wide and far out onto the subaerially exposed shelf with limited fluvial

incision, which is supported by the limited erosional relief associated with the unconformities in the Wilhelmøya Subgroup (Rismyhr et al., 2018).

3. Methods

3.1 TOC and organic $\delta^{13}C$ measurements

All samples were measured for Total Organic Carbon (TOC) content and organic $\delta^{13}C$ following the standard protocol of Utrecht University. The samples were freeze-dried and powdered, after which 1 g of powdered samples were treated twice using 25 ml 1M HCl and rinsed twice with de-ionized water to remove carbonates. Samples were dried in a 60 °C oven for 72 hours and homogenised. The prepared samples were analysed for carbon content with a Flash IRMS Elemental Analyzer from a Thermo Scientific EA IsoLink IRMS System at the department of Earth Sciences at Utrecht University. The TOC values were calculated by multiplying the measured carbon content with the ratio of the decarbonated and original sample weights. Based on the resulting carbon content values, decarbonated residues containing 30-40 µg of organic carbon were analysed for organic $\delta^{13}C$. Organic $\delta^{13}C$ measurements were performed at the department of Earth Sciences at Utrecht University using the full system of a Thermo Scientific EA IsoLink IRMS System; consisting of a Flash IRMS Elemental Analyzer, Delta V IRMS and Conflo IV Universal Interface. The $\delta^{13}C$ measurements resulted in a second carbon content percentage for every sample. The final TOC results were calculated by taking the average of the first and second carbon content measurements.

3.2 Petrographic thin sections

Petrographic thin sections were made from the samples with larger grainsizes, phosphate nodules and siderite cementation by Leonard Bik at Utrecht University. Using these thin sections the samples could be analysed for lithological content using an optical microscope. In thin sections where phosphatic (coated) grains were present the quantity was determined by counting through the long side of the thin sections 3 times at 10x magnification.

3.3 Palynological preparation and quantification

The samples with finer grain sizes (mostly shales, some siltstones and sandstones) were used for palynological analysis; shale samples were prioritized, as the palynomorphs are likely to be best preserved in these sediments. Around 15 g of sample material was crushed and *Lycopodium* tablets were added for absolute quantification. Crushed samples were prepared following standard palynological protocol at Utrecht University. Carbonates were removed and *Lycopodium* tablets were dissolved by adding 10% HCl, and 30% HCl for samples with more carbonate content. Siliciclastic elements were removed by processing twice with 38% HF. Every HF step was followed by 30% HCl treatment to prevent CaF_2 precipitation. The remaining material was sieved with a 10 µm nylon-mesh and residues were permanently mounted on glass slides using 5% Polyvinyl Alcohol (PVA) solution and UV glass glue. The palynomorphs mounted on the glass slides were analysed using an optical microscope. The preservation in the samples is on average quite poor, and a large difference in quality between samples was observed. In some samples large diversities are well-preserved, while in other samples the preservation is too poor to perform a reliable quantitative analysis. On samples with sufficient preservation palynomorphs were counted (~64% of samples),

reaching 200-300 palynomorphs per sample. Samples with poor preservation were analysed qualitatively. 4 samples were found to be barren and were not further analysed. Palynomorphs that could be recognized as spores, pollen or dinocysts but not assigned to a taxon due to preservation were counted as an indeterminable specimen of their group (noted as 'group' indet.). This way the ratio of pollen/spores/dinocyst could still be determined accurately. The samples were checked for possible aberrant pollen/spores. One sample from an interval above the snow covered area at Festningen was prepared for palynological analysis. This one sample was found to be barren, however, meaning the focus of this study is completely on the lower Knorringfjellet Formation samples.

4. Results

4.1 TOC and $\delta^{13}C_{org}$

$\delta^{13}C_{org}$ measurements show background values between -25 and -24.3‰ (VPDB; Vienna Pee Dee Belemnite) and multiple excursions to more negative values. A large ~-3.8‰ CIE is found from 1.6 to 4.9 m height, with values dipping as low as -28 to -29.3‰. This excursion correlates with the coarser, phosphate rich sediments of the Slottet Bed. Two smaller negative $\delta^{13}C_{org}$ excursions with values below -25‰ are found at 7-7.5 m (~-1‰) and 11.1-12 m height (~-1.7‰). Furthermore, two samples at 9.22 m and 10.3 m height show slightly more negative values than the surrounding samples.

The TOC results vary between 0.14 and 1.5 weight%, with an average of 0.70%. Most shale samples contain relatively high TOC, ranging from 1.0 to 1.5%. Lower TOC values (mostly 0.2-0.6%) correlate with the coarser lithologies associated with shallower water depths. The $\delta^{13}C_{org}$ and TOC values show a moderate positive correlation, $r = .68$, $p < .00001$. The coarser-grained samples with lower TOC values also show lighter $\delta^{13}C_{org}$ values in most samples. The negative $\delta^{13}C_{org}$ excursion at the top of the section is the only excursion to show lighter values in the fine-grained shale samples as well.

4.2 Thin section analysis

The lithology of the coarse-grained samples selected for thin sections is mostly dominated by subangular to subrounded quartz grains. Presence of phosphate is indicated by brown grains and microsparitic cement that is found in the samples from the bottom of the Slottet Bed up until 9 m in the section. In almost all samples black pyrite grains can be observed; usually small and at most covering a few percentages of the total area.

The Slottet Bed contains well-rounded phosphate nodules with a diameter of up to ~5 cm. Thin sections reveal also microscopic brown phosphatic grains are mostly found in the Slottet Bed, at 1.6-4.4 m height (appendix 1), coinciding with the largest negative CIE. In most samples these take the form of brown elliptical grains without coating. Phosphatic coated grains are mostly found in three samples at the bottom and middle of the Slottet Bed; FT23/4, FT23/10 and FT23/11 at 1.675, 2.9 and 3.05 m height, respectively (figure 4). In sample FT23/11, at 3.05 m height, a lot of quartz grains show a very thin phosphatic coating as well. In two other samples, at 2.45 and 3.35 m height, only a few poorly defined coated grains could be observed. The sample at the top of the Slottet Bed (4.375 m) has no coated grains, although it contains a larger amount of brown phosphate grains without clear coating. The well-developed coatings and intact state of the phosphatic coated grains at the bottom of the Slottet Bed indicate the coated grains were formed while this conglomerate was deposited. In sample FT23/10 in the middle of the Slottet Bed (2.9 m) the coated grains are

often fragmented and less clearly coated, suggesting these might be reworked grains from the conglomerate at the bottom of the bed. In sample FT23/11 (3.05 m) the coated grains are better preserved again, although not as well-defined as at the bottom of the Slottet Bed. This was likely a second phase of phosphatic coated grains formation.

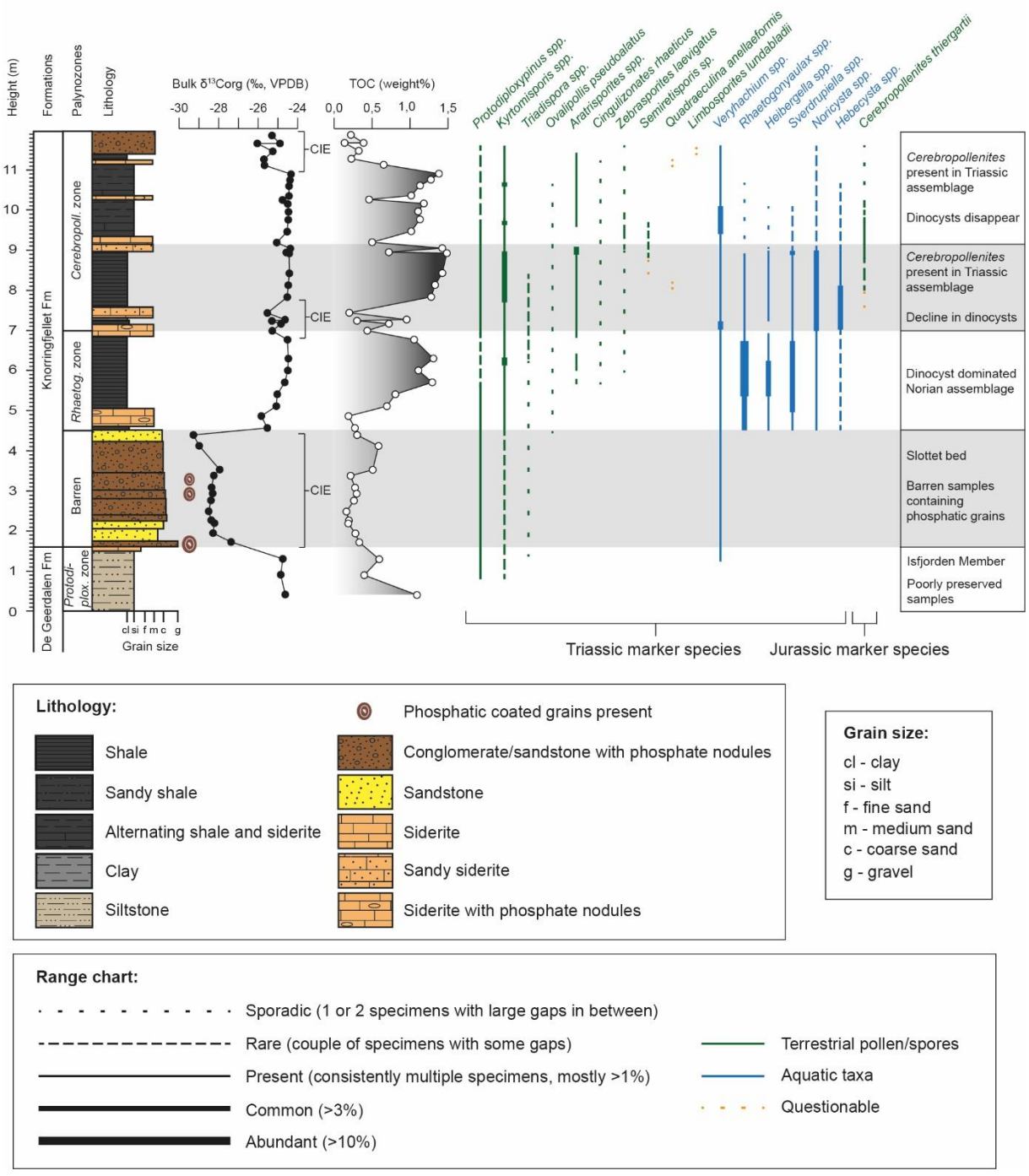

Figure 3: Combined stratigraphic, geochemical and palynological data. The palynological zones described in this study are shown. A stratigraphic column shows the lithologies and grain sizes of the Festningen section, and locations of phosphatic coated grains are marked. $\delta^{13}C_{org}$ and TOC results are given in ‰VDPB and weight%, respectively. Carbon isotope excursions (CIEs) are indicated. A selected range chart highlights the marker species occurrences, from sporadic to abundant (see appendix 2 for a full range chart of all recognised taxa that occurred at least sporadically).

The phosphatic coated grains vary from a spherical to an elliptical shape and range from 150 to 400 µm in size, most commonly sized around 300 µm. The nuclei of the coated grains are usually composed of quartz grains, or the grains seem to be purely formed by phosphate. The cortices of the coated grains consist of concentric phosphatic laminae. These laminae alternate between lighter layers; white quartz or light brown phosphate, and darker layers; dark brown phosphate or black pyrite. The laminae generally replicate the shape of the nucleus. In some coated grains the laminae are partly remineralized and form a less structured mix of phosphate, quartz and pyrite. Mostly in the samples in the middle of the Slottet Bed (2.9-3.05 m) the phosphate grains are partly pyritized. In some phosphate rich samples larger areas dominated by phosphate are found within the thin section, which might be multiple unclear phosphate grains clumped together (i.e. figure 4; far right picture of sample FT23/10). The samples at the top of the section, above 9 m, do not contain any phosphatic grains and have a more white matrix, not showing indication of phosphate presence.

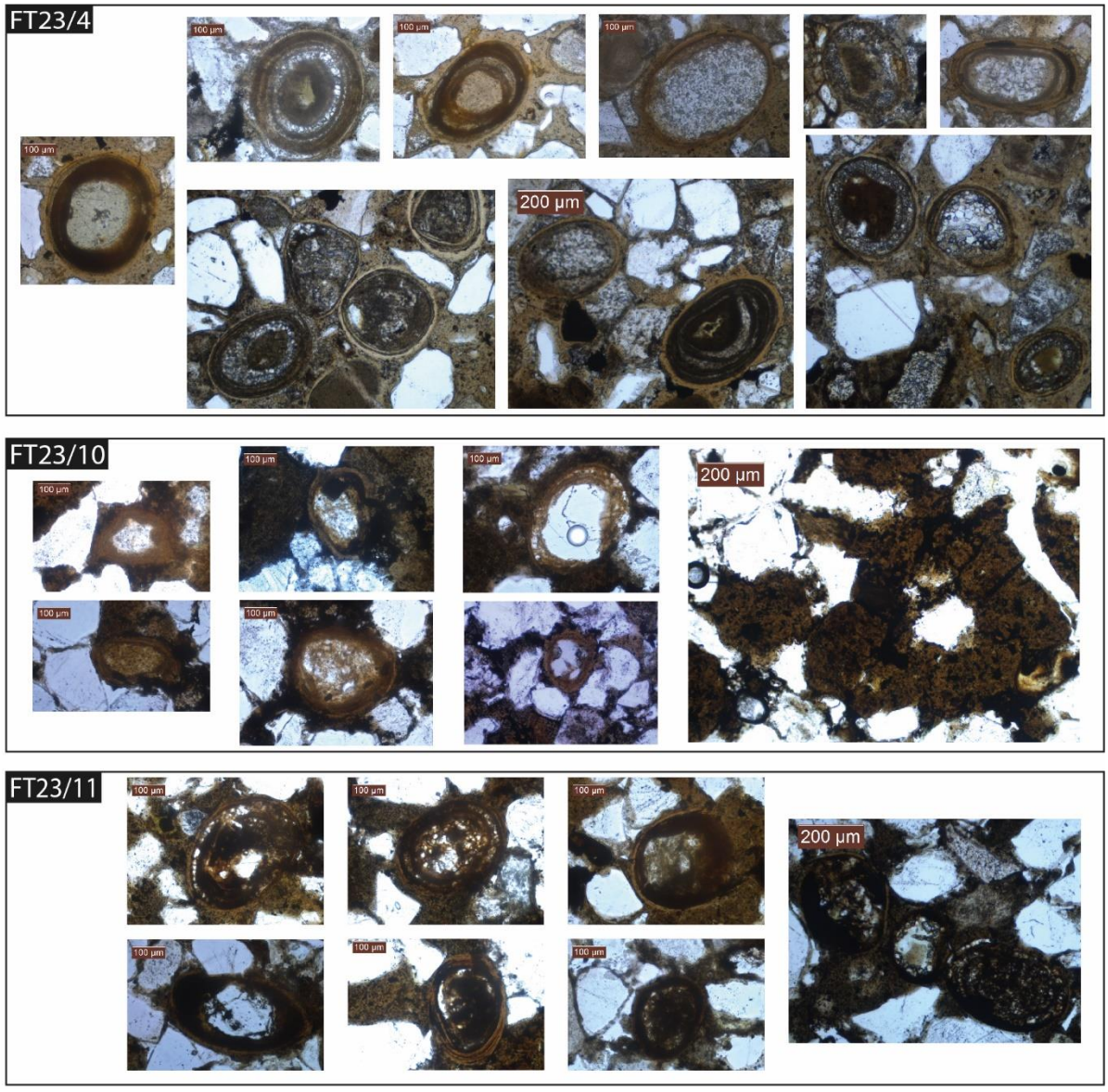

Figure 4: Photomicrographs of phosphatic coated grains found in petrographic thin sections. Phosphatic coated grains were found in samples FT23/4 (height: 1.675 m), FT23/10 (height: 2.9 m) and FT23/11 (height: 3.05 m). All photos are displayed at the same scale.

4.3 Palynology

4.3.1. Marker species biostratigraphy

Based on the occurrence of palynological marker species the studied section can be divided into three palynological zones (figure 3). At the top of the Isfjorden Member from the De Geerdalen Formation, just below the Slottet Bed, samples do not show a good preservation, therefore no quantitative analysis was performed here. However, a qualitative analysis showed *Protodiploxypinus spp.* were relatively abundant (see plate 1 for photomicrographs of pollen taxa). Therefore, this section is labelled *Protodiploxypinus* zone similar to earlier research in the area (Paterson & Mangerud, 2015; Rismyhr et al., 2018). The pollen taxon *Chasmatosporites spp.*, spore taxa *Deltoidospora spp.* and *Concavisporites spp.* (see plate 2 and 3 for photomicrographs of spore taxa) and the acritarch *Veryhachium sp.* are also recognized here (figure 5); these taxa are consistently present in the complete studied section. Samples from the Slottet Bed proved to be barren; in only one sample, at the top of the bed, some taxa could be recognized qualitatively. Because of this, no palynological zone is assigned to this part of the section.

Starting above the Slottet Bed, a diverse assemblage dominated by dinocysts is found in the lower part of the Knorringfjellet Formation. Typical Triassic dinocyst taxa that occur include *Rhaetogonyaulax spp.*, *Heibergella spp.*, *Sverdrupiella spp.*, *Noricysta spp.* and *Hebecysta sp*. (plate 4). *Rhaetogonyaulax spp.* is the most common and is reduced to very low abundance at 7 m in the section, making it the most logical taxa to title the zone from 4.5-7 m height. The Triassic pollen and spore taxa *Kyrtomisporis spp.*, *Ovalipollis pseudoalatus*, *Protodiploxipinus spp.* and *Triadispora spp.* are recognized throughout this whole zone, *Aratrisporites spp.*, *Cingulizonates rhaeticus* and *Zebrasporites laevigatus* start to be recognized just under 6 m in the section.

The next palynological zone is characterized by an overall decrease in dinocyst abundance due to a strong decline of *Rhaetogonyaulax spp.*, *Heibergella spp.* and *Sverdrupiella spp.*, although *Noricysta spp.* and *Hebecysta sp.* are actually found more commonly. *Cerebropollenites thiergartii*, a species commonly regarded as a marker for the base of the Jurassic, is found in the section starting around 8 m height. The Triassic marker taxa *Semiretisporis sp.* (most likely *gothae*) is also recognized in this part of the section, and *Kyrtomisporis spp.* and *Aratrisporites spp.* become more common. Above 9 m height there is a second decline in dinocysts, with *Noricysta spp.* and *Hebecysta sp.* now reduced in abundance as well. Triassic marker species *Quadraeculina anellaeformis* and *Limbosporites lundabladii* are not recognized very convincingly, besides some questionable occurrences. This upper zone is not characterized by one very common or dominant taxa, therefore it was decided to label this interval *Cerebropollenites* zone, as this is the most remarkable taxa observed in this zone. The top two samples above 9 m height were solely analysed qualitatively. Most terrestrial Triassic marker species were still observed in these samples, and no new Jurassic marker species were identified.

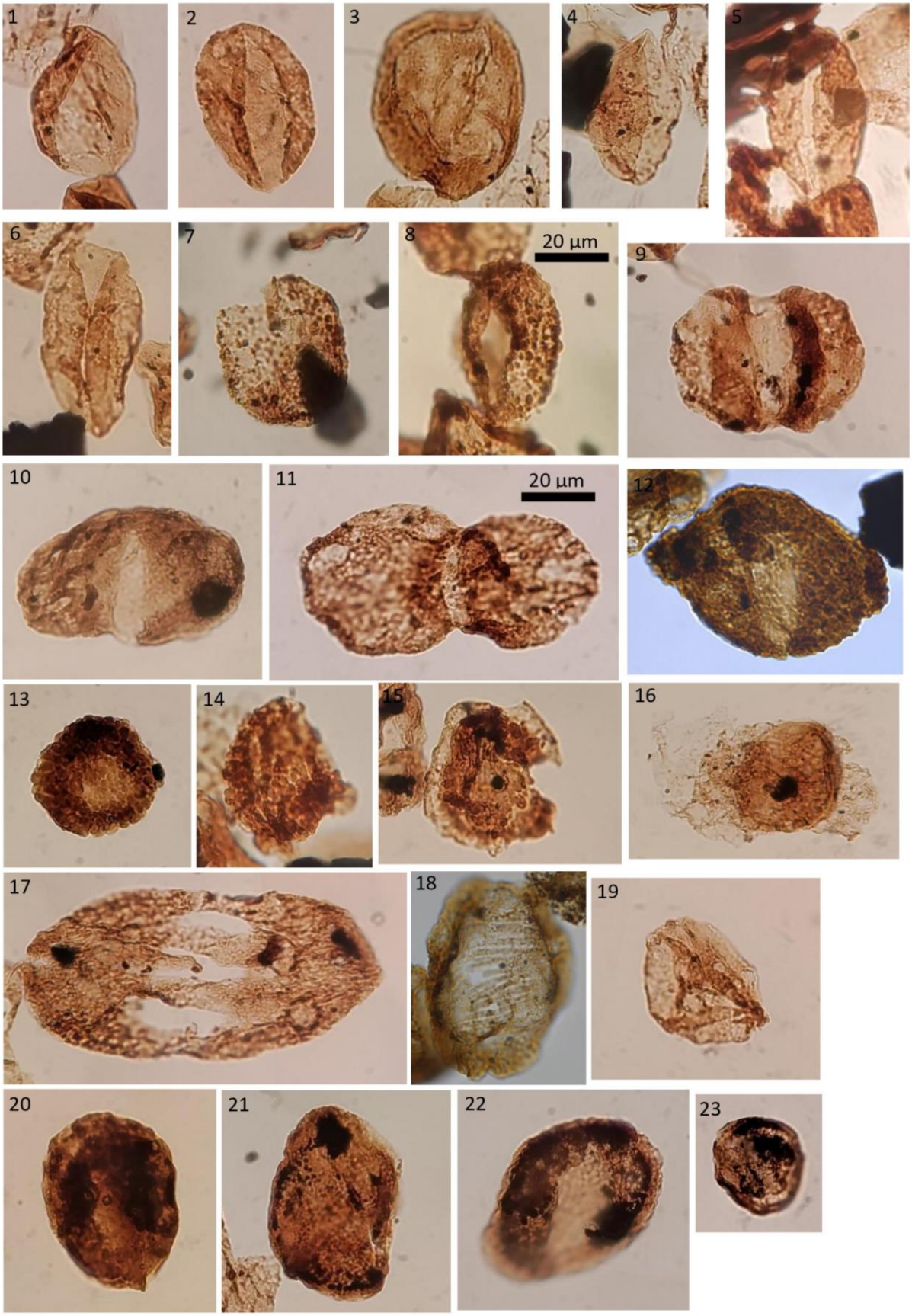
1
2
3
4
5
6
7
8
20 µm
9
10
11
20 µm
12
13
14
15
16
17
18
19
20
21
22
23

Plate 1. Various encountered pollen grains:

1. *Chasmatosporites elegans* (FT23/22; 6.3 m height)

2. *Chasmatosporites hians* (FT23/29; 7.85 m height)

3. *Chasmatosporites magnolioides* (FT23/22; 6.3 m height)

4. *Monosulcites punctatus* (FT23/22; 6.3 m height)

5. *Monosulcites sp. (minimus*?) (FT23/22; 6.3 m height)

6. *Ovalipollis pseudoalatus* (FT23/31; 8.45 m height)

7. *Cerebropollenites*/*Sciadopityspollenites thiergartii* (FT23/30; 8.15 m height)

8. *Cerebropollenites*/*Sciadopityspollenites thiergartii* (FT23/37; 9.8 m height)

9. *Alisporites sp.* (FT23/34; 9.08 m height)

10. *Alisporites sp.* (*radialis*?) (FT23/22; 6.3 m height)

11. *Alisporites sp.* (FT23/34; 9.08 m height)

12. *Protodiploxypinus gracilis* (FT23/22; 6.3 m height)

13. *Protodiploxypinus decus* (FT23/48A; 11.73 m height)

14. *Protodiploxypinus minor*? (FT23/22; 6.3 m height)

15. *Triadispora verrucata* (FT23/34; 9.08 m height)

16. *Triadispora sp.* (*verrucata*?) (FT23/22; 6.3 m height)

17. *Lunatisporites rhaeticus* (FT23/34; 9.08 m height)

18. *Striatoabieites multistratus* (FT23/22; 6.3 m height)

19. *Araucariacites australis* (FT23/29; 7.85 m height)

20. *Podosporites sp.* (FT23/27; 7.28 m height)

21. *Porcellispora longdonensis* (FT23/34; 9.08 m height)

22. *Quadraeculina anellaeformis*? (FT23/30; 8.15 m height)

23. *Granuloperculatipollis rudis*? (FT23/19; 5.4 m height)

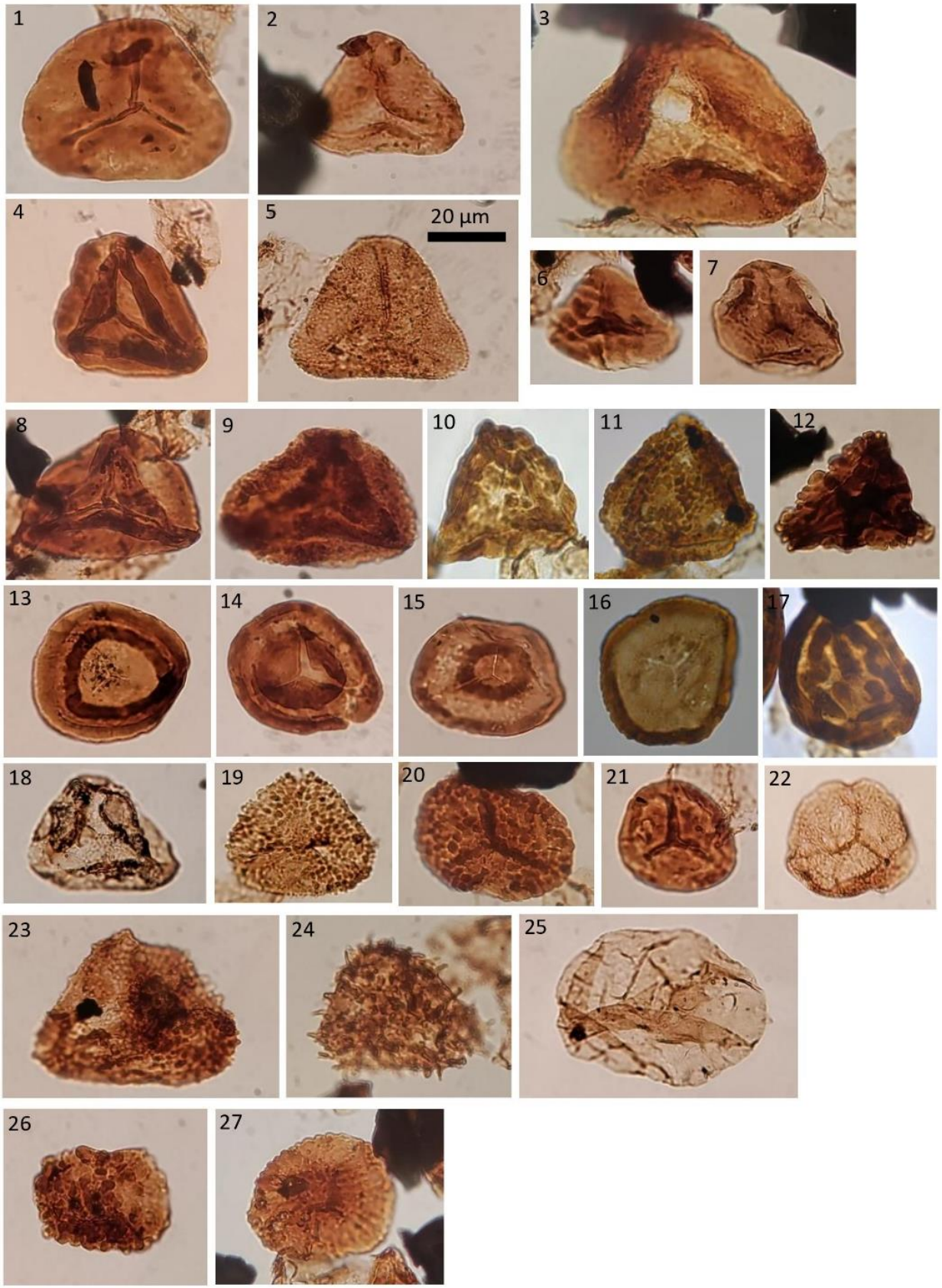
1
2
3
4
5
20 µm
6
7
8
9
10
11
12
13
14
15
16
17
18
19
20
21
22
23
24
25
26
27

Plate 2. Encountered spore taxa:

1. *Deltoidospora toralis* (FT23/23)

2. *Deltoidospora mesozoica*? (FT23/22; 6.3 m height)

3. *Concavisporites scabratus* (FT23/22; 6.3 m height)

4. *Concavisporites crassiexinius* (FT23/31; 8.45 m height)

5. *Trachysporites fuscus* (FT23/22; 6.3 m height)

6. *Zebrasporites interscriptus* (FT23/22; 6.3 m height)

7. *Zebrasporites laevigatus* (FT23/39; 10.2 m height)

8. *Kyrtomisporis laevigatus* (FT23/34; 9.08 m height)

9. *Kyrtomisporis moerki* (FT23/34; 9.08 m height) – recently defined by Paterson and Mangerud (2020)

10. *Kyrtomisporis gracilis* (FT23/22; 6.3 m height)

11. *Kyrtomisporis speciosus* (FT23/22; 6.3 m height) – similar to Paterson et al. (2019) plate 1-28

12. *Kyrtomisporis speciosus* (FT23/39; 10.2 m height) – similar to Vigran et al. (2014) plate 8-E

13. *Polycingulatisporites spp.* (FT23/29; 7.85 m height)

14. *Polycingulatisporites bicollateralis* (FT23/21; 6 m height)

15. *Annulispora folliculosa* (FT23/31; 8.45 m height)

16. *Stereisporites sp.* (FT23/22; 6.3 m height)

17. *Striatella seebergensis* (FT23/22; 6.3 m height)

18. *Converrucosisporites cameroni* (FT23/19; 5.4 m height) - similar to Lindström et al. (2023) plate 1-26

19. *Converrucosisporites cameroni*? (FT23/23; 6.78 m height) – similar to Lindström et al. (2023) plate 2-11 and 12

20. *Lycopodiacidites rugulatus* (FT23/30; 8.15 m height)

21. *Camarozonosporites rudis*? (FT23/32; 8.95 m height)

22. *Baculatisporites wellmanii* (FT23/21; 6 m height)

23. *Clathroidites papulosus* (FT23/23; 6.78 m height)

24. *Acanthotriletes varius* (FT23/29; 7.85 m height)

25. *Calamospora sp.* (FT23/48A; 11.73 m height)

26. *Verrucosisporites sp.* (FT23/19; 5.4 m height)

27. *Radisporis costasus* (FT23/37; 9.8 m height)

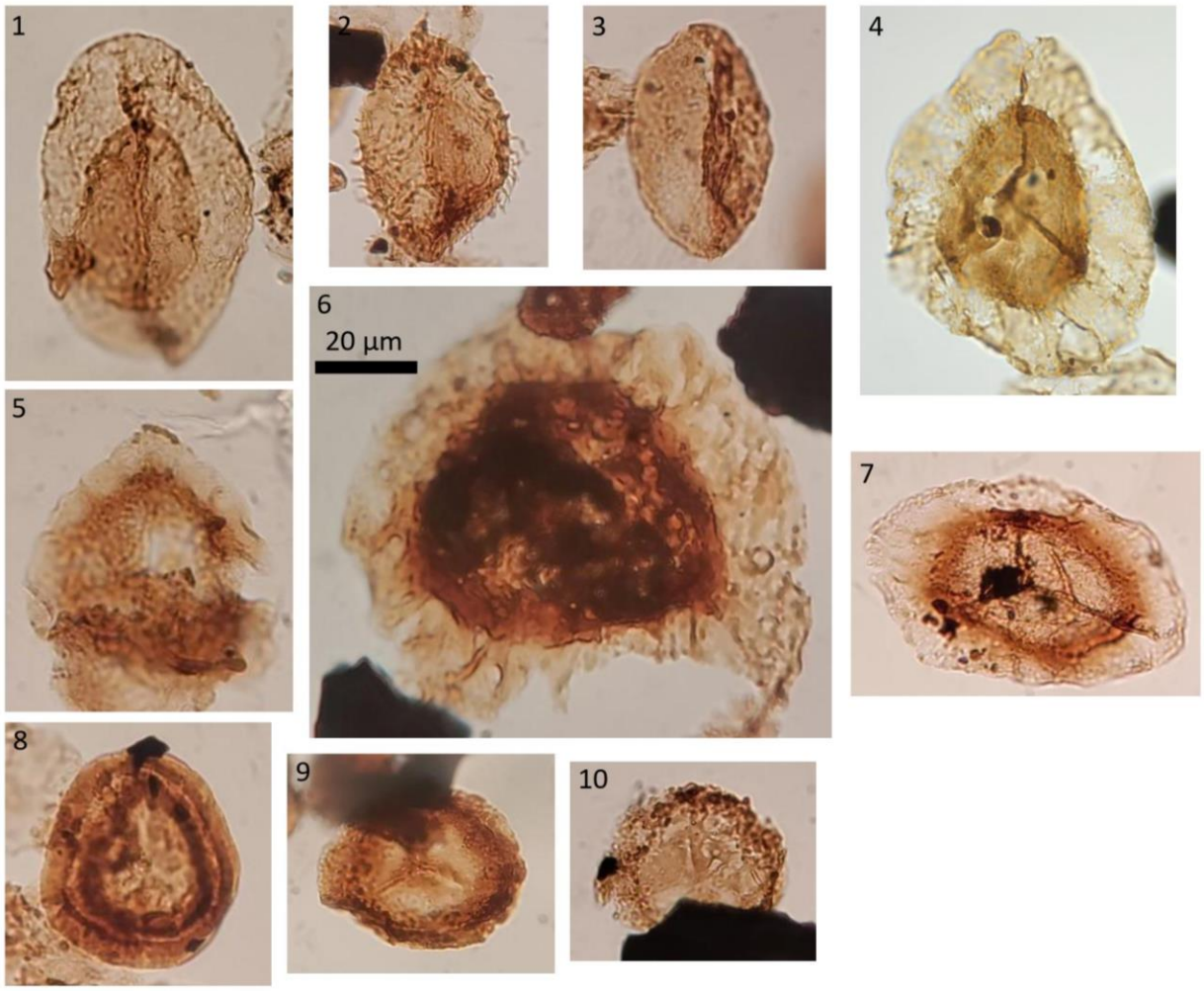

Plate 3. Encountered Lycopodiopsida spore taxa:

1. *Aratrisporites macrovatus* (FT23/22; 6.3 m height)
2. *Aratrisporites palletae* (i.e. Paterson & Mangerud, 2017 plate IV-F) or *fimbratus* (i.e. Lindstrom et al. 2023 plate 2-16) (FT23/22; 6.3 m height)
3. *Aratrisporites laevigatus* (FT23/22; 6.3 m height)
4. *Velosporites cavatus*? (FT23/22; 6.3 m height)
5. *Limbosporites lundbladii*?? (FT23/48A; 11.73 m height)
6. *Semiretisporis sp.* (*gothae*?) (FT23/37; 9.8 m height)
7. *Cingulizonates rhaeticus* (FT23/34; 9.08 m height)
8. *Densosporites sp./Densoisporites sp.* (FT23/22; 6.3 m height)
9. *Densosporites cerebralis* (FT23/20; 5.7 m height)
10. *Uvaesporites reissingerii*? (FT23/32; 8.95 m height)

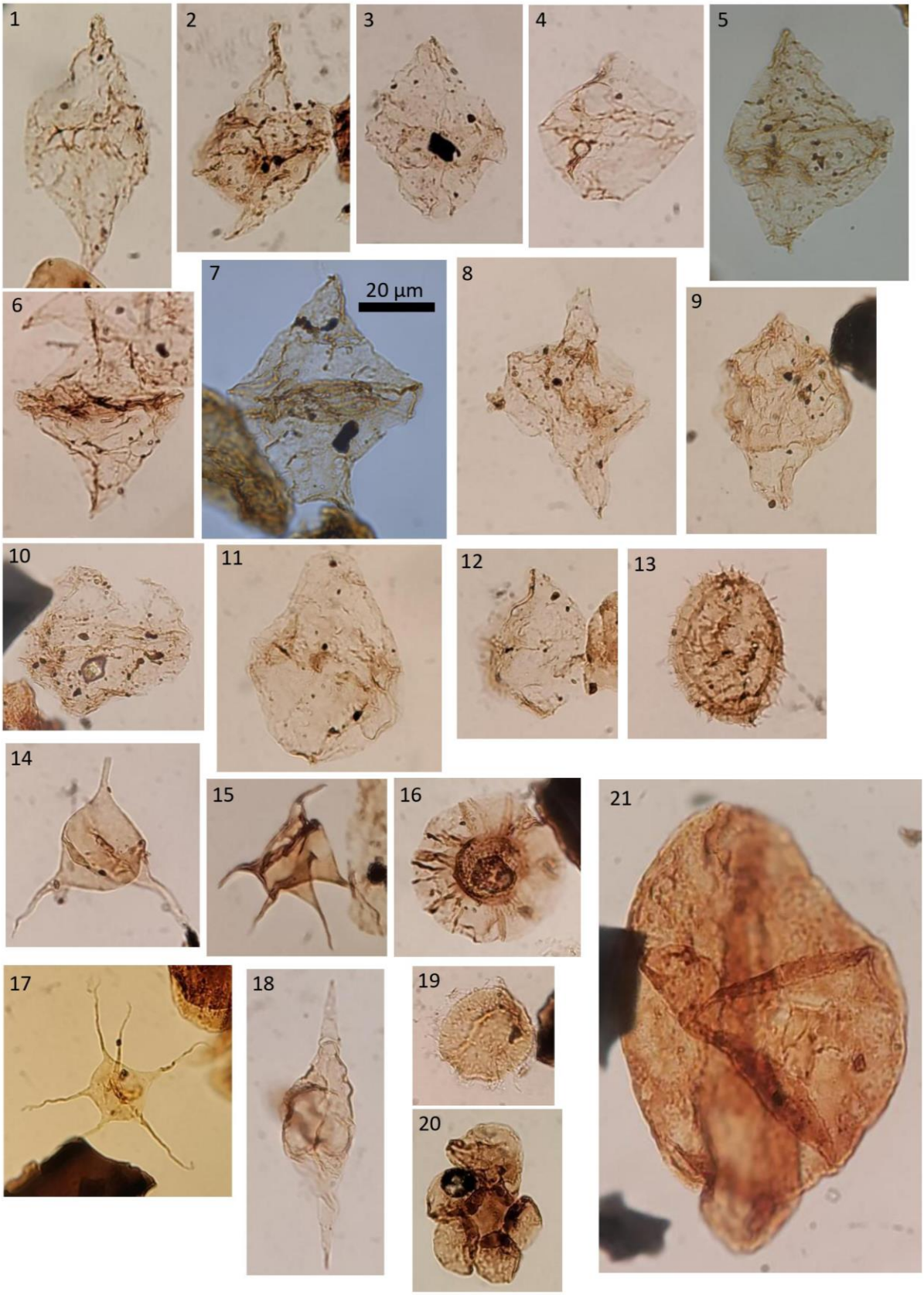
1
2
3
4
5
6
7
20 µm
8
9
10
11
12
13
14
15
16
21
17
18
19
20

Plate 4. Various aquatic taxa; dinoflagellate cysts (1-13) , acritarchs (14-18), prasinophyte (19) and microforaminiferal tests (20-21):

1. *Rhaetogonyaulax sp.* (*rhaetica*?) (FT23/22; 6.3 m height)
2. *Rhaetogonyaulax sp.* (FT23/22; 6.3 m height)
3. *Heibergella aculeata* (FT23/30; 8.15 m height)
4. *Heibergella asymmetrica* (FT23/18; 5.1 m height)
5. *Heibergella salebrosace* (FT23/22; 6.3 m height)
6. *Sverdrupiella baccata* (FT23/22; 6.3 m height)
7. *Sverdrupiella sp.* (*cristata*?) (FT23/22; 6.3 m height)
8. *Sverdrupiella sp.* (*spinosa/baccata*?) (FT23/22; 6.3 m height)
9. *Sverdrupiella mutabilis* (FT23/34; 9.08 m height)
10. *Noricysta sp.* (FT23/34; 9.08 m height)
11. *Hebecysta sp.* (FT23/32; 8.95 m height)
12. *Shublikodinium arcticum* (FT23/30; 8.15 m height)
13. *Beaumontella sp??* (FT23/27; 7.28 m height)
14. *Veryhachium sp.* (FT23/27; 7.28 m height)
15. *Baltisphaeridium sp.*? (FT23/25; 7.18 m height)
16. *Pterospermella sp.* (FT23/27; 7.28 m height)
17. *Dorsennidium simplex* (FT23/22; 6.3 m height)
18. *Leiofusa jurassica*? (FT23/37; 9.8 m height)
19. *Cymatiosphaera* sp.? (FT23/3; 1.25 m height)
20. Microforaminiferal test lining (FT23/29; 7.85 m height)
21. Microforaminiferal test lining?? (FT23/29; 7.85 m height)

4.3.2. Palynological trends

The relative abundances of the most important encountered taxa were determined for the interval where preservation allowed for a quantitative analysis (figure 5). For the intervals that were not counted + signs indicate observed presence of the taxa. The relative abundances of most pollen taxa remain very constant over the counted interval. *Chasmatosporites spp.* consistently occur commonly. The most prominent changes are an increase in abundance of *Araucariacites australis* from 7.2 to 9 m height and *Cerebropollenites thiergartii* coming in at 8 m height. Although *C. thiergartii* is found at low abundances of ~0.5-2% of the total counts, it is recognized consistently in the upper part of the section.

The abundance of indeterminable trilete spores is higher in the bottom meter and top 1.5 meter of the counted section. This is likely the result of poorer preservation in these samples, as the amount of indeterminable pollen counted in these samples is slightly higher as well. *Deltoidospora spp.*, *Concavisporites spp*. and *Kyrtomisporis spp*. are the most dominant spore taxa. *Concavisporites spp*. abundance is very consistent throughout the section, *Deltoidospora spp.* abundance does show a peak, mostly from 7 to 8.5 m height. *Kyrtomisporis spp.* are found more commonly in the upper interval as well. All other spore taxa occur comparatively rare; no higher than 2% of the total counts. The spore/pollen ratio remains stable throughout the section; with values mostly ranging between 0.52 and 0.66 (total spores/(total pollen + total spores)).

In the lower part of the section *Rhaetogonyaulax* spp. is by far the most dominant dinocyst taxa with relative abundances up to 24%, followed by *Sverdrupiella spp.* (up to 13%) and Heibergella spp. (up to 10%), all of which are decreased to a few percent of the assemblage above 7 m height. *Noricysta spp.* and *Hebecysta sp.* abundance peaks from 7 to 9 m height, while above 9 m height *Veryhachium sp.* becomes the by far most dominant aquatic taxa.

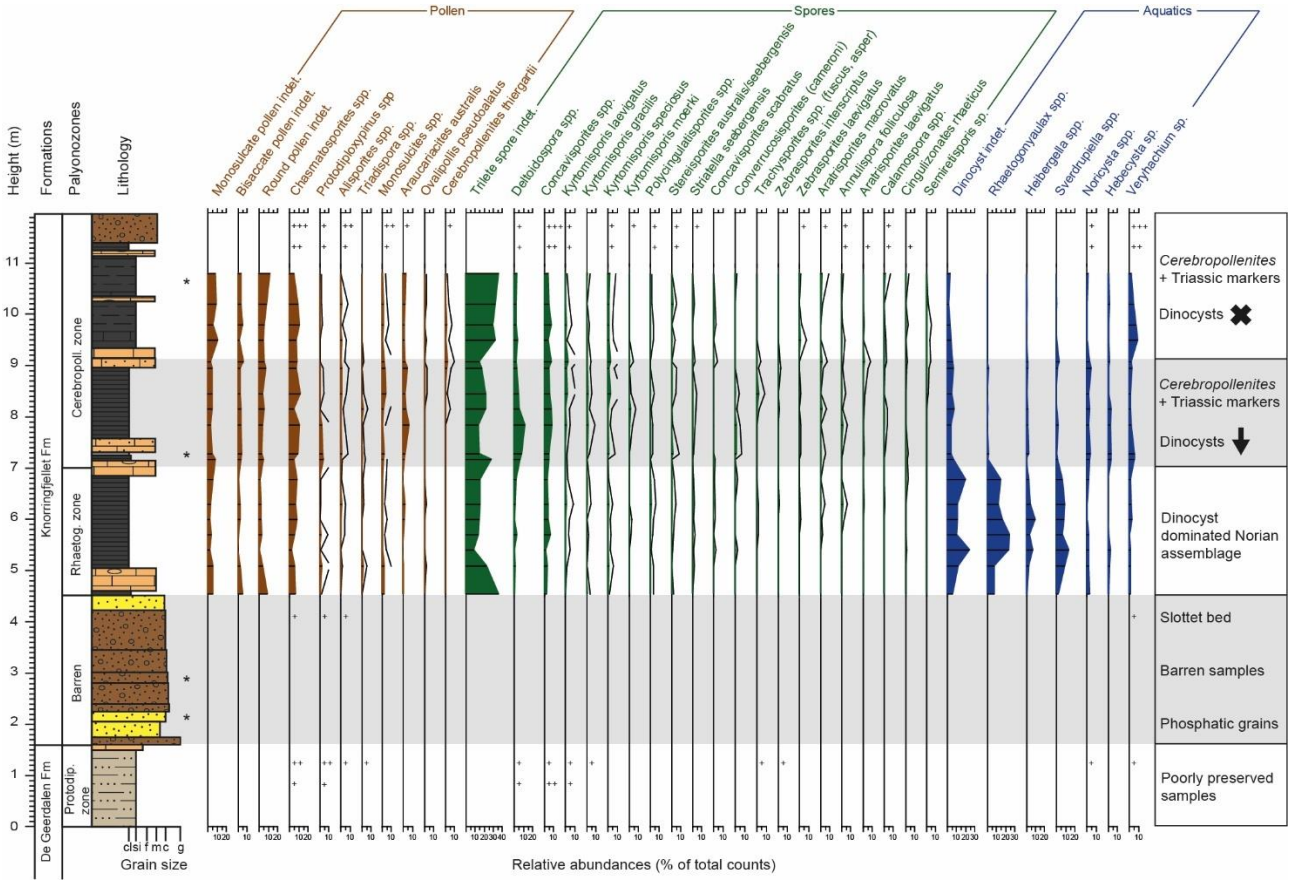

*Figure 5: Relative abundances of the most important encountered taxa as a percentage of the total counts. Taxa appearing very sporadically were not included in this figure. The intervals below 4.5 m and above 11 m were not suitable for relative abundance counts; + symbols here indicate presence of identified taxa (+: 1-2 specimens, ++: common +++: very common/dominant). Samples prepared for palynological analysis that were found to be barren are indicated by a *.*

Based on the known botanical affinities of the taxa that were recognized (table 1), the relative abundances of the most dominant floral groups can be reconstructed (figure 6). Ferns are the most dominant plant group throughout the section, followed by cycads/ginkgos and conifers. Mosses and club mosses are found more inconsistently and at much lower abundances. Seed ferns and horsetails do not present a large part of the assemblage, as these groups are only represented by *Alisporites spp.* and *Calamospora spp.*, respectively.

Table 1: Table with botanical and ecological affinities for relevant taxa. Affinities are mostly derived from Lindström (2016), Lindström, Erlström, et al. (2017) and Bos et al. (2023). Supplementary sources are cited in the table.

Palynofloral taxon	Botanical affinity	Parent group	Habit	Preferred environment	Climatic preferences
Pollen species					
Chasmatosporites sp.	Cycadopsida/ Ginkgopsida, Cycadales/ Ginkgoales	Cycads/ Ginkgos	Canopy	Lowland (Abbink, 1998), mire	Drier, cooler (Abbink, 1998)
Monosulcites sp.	Cycadopsida/ Ginkgopsida, Bennettitales/Peltaspermales	Cycads/Ginkgos (seed ferns)	Canopy	Mire, drier patches	Drier (Abbink, 1998)
Alisporites sp.	Coniferales/	Seed ferns	Upper canopy	Lowland, mire	Hygrophytic

	Corystospermales, Corystospermaceae				
Cerebropollenites thiergartii	Coniferales, Taxodiaceae	Conifers	(Upper) canopy/ shrubs	?Pioneer, well-drained	
Protodiploxypinus sp.	Coniferales	Conifers	Canopy	Well-drained	Xerophytic
Triadispora sp.	Coniferales/Voltziales, Voltziaceae	Conifers			Xerophytic
Araucariacites australis	Coniferales, Araucariaceae	Conifers	canopy/shrubs	Coastal (Abbink, 1998)	Cooler (Abbink, 1998)
Lunatisporites spp.	Coniferales	Conifers	Upper canopy	Well-drained	Xerophytic
Striatoabieites spp.	Coniferales	Conifers			Xerophytic
Granuloperculatipollis rudis	Coniferales, Cheirolepidiaceae	Conifers	Upper canopy	Coastal, well-drained	Warm conditions
Quadraeculina anellaeformis	Coniferales, Podocarpaceae	Conifers	Canopy/shrubs	Upland, well-drained	Xerophytic
Ovalipollis pseudoalatus	nd?		Unknown?		
Spore taxa					
Deltoidospora spp.	Pteridopsida/ Filicopsida, Filicales, Dipteridaceae/Dicksoniaceae	Ferns	Understory, ground cover	Pioneer, drier patches in mire	Drier, warmer (Abbink, 1998)
Concavisporites sp.	Pteridopsida/ Filicopsida, Filicales, Dipteridaceae/Matonicaeae	Ferns	Understory, ground cover	Lowland, drier environments	Hygrophytic
Kyrtomisporis spp.	Polypodiopsida /Pteridopsida/ Filicopsida	Ferns (Mädler, 1964)			
Striatella seebergensis	Pteridopsida/ Filicopsida, Polypodiales, Polypodiaceae	Ferns	Ground cover	Mire	Hygrophytic
Zebrasporites laevigatus/interscriptus	Pteridopsida/ Filicopsida, Filicales	Ferns	Understory, ground cover	Lowland, mire	Hygrophytic
Trachysporites fuscus	Pteridopsida/ Filicopsida	Ferns	Understory, ground cover	Lowland	Hygrophytic
Converrucosisporites spp.	Pteridopsida/ Filicopsida	Ferns	Ground cover	Lowland, mire	Hygrophytic
Lycopodiacidites rugulatus	Pteridopsida/ Filicopsida	Ferns	Ground cover	Mire	Hygrophytic
Baculatisporites wellmanii/comaumensis	Pteridopsida/ Filicopsida, Filicales, Osmundaceae	Ferns	Understory, ground cover	Lowland, mire	Wetter, warmer (Abbink, 1998)
Acanthotriletes varius	Pteridopsida/ Filicopsida	Ferns	Understory, ground cover		
Camarozonosporites spp.	Pteridopsida/ Filicopsida	Ferns	Ground cover	Mire	
Conbaculatisporites spp.	Pteridopsida/ Filicopsida, Filicales, Dipteridaceae	Ferns	Understory/ ground cover	Lowland	Hygrophytic
Polycingulatisporites spp.	Bryophyta	Mosses	Ground cover	Lowland, mire, river banks or wet environments	Hygrophytic
Annulispora folliculosa	Bryophyta	Mosses	Ground cover	Mire	
Stereisporites spp.	Bryophyta, Sphagnopsida, Sphagnidae, Sphagnaceae	Mosses	Ground cover	Lowland, mire, river banks or wet environments	Hygrophytic
Aratrisporites spp.	Lycopodiopsida	Clubmosses	Ground cover	Coastal, mire	Xerophytic (Retallack, 1975)
Cingulizonates rhaeticus	Lycopodiopsida	Clubmosses	Ground cover	Lowland, mire	Hygrophytic
Limbosporites lundbladii	Lycopodiopsida	Clubmosses	Ground cover	Lowland, mire or wet environments	Hygrophytic
Densosporites spp.	Lycopodiopsida, Selaginellales	Clubmosses	Ground cover	Mire	Hygrophytic
Calamospora tener	Equisetopsida, Equisetales, Equisetaceae	Horsetails	Ground cover	River banks, mire, lake shores	Tropical to temperate (Abbink, 1998)
Semiretisporis sp.	nd				

Cycads/Ginkgos are a constant important factor throughout the assemblage. Mosses and seed ferns similarly do not show any significant peaks in abundance. Ferns show higher abundances in the *Cerebropollenites* zone, however relative to the terrestrial counts there is only a slight peak at 7.8 to 8.5 m height. Conifers are the most dominant in the interval from 7-9 m. Here they peak relative to the terrestrial counts as well; ~10% of the terrestrial counts, compared to ~5% in the *Rhaetogonyaulax* zone and upper part of the *Cerebropollenites* zone. Horsetails are almost exclusively found in the *Cerebropollenites* zone, and club mosses are also more common in this zone compared to the *Rhaetogonyaulax* zone.

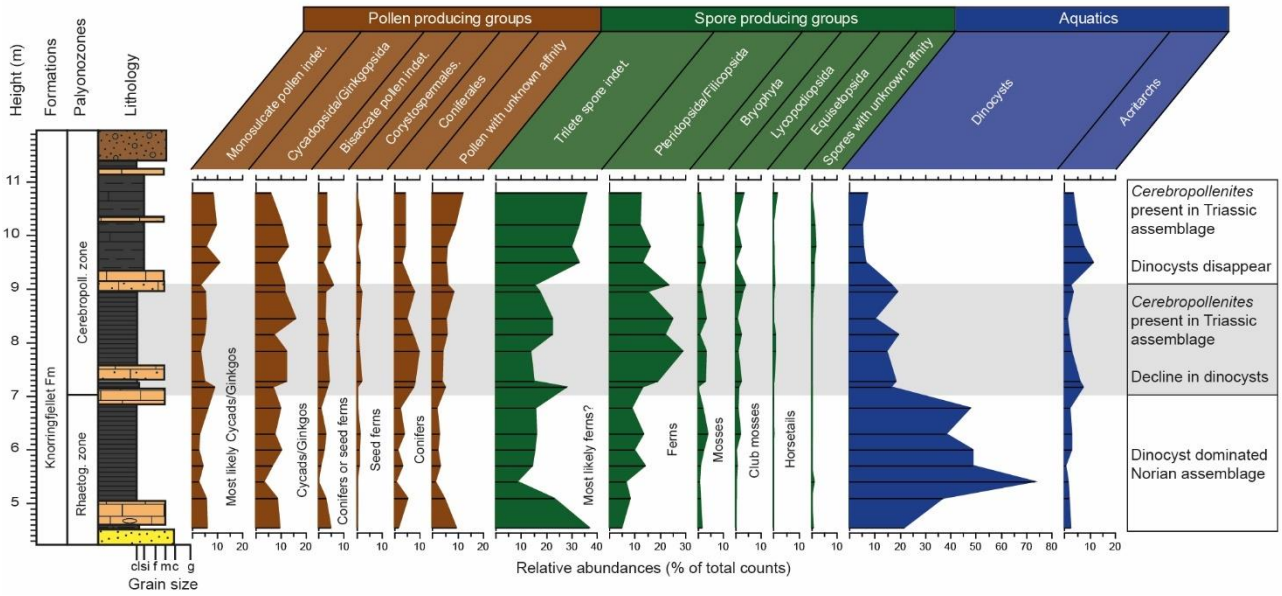

Figure 6: Vegetational reconstruction showing the major aquatic groups and most dominant floral groups as inferred from botanical affinities of counted taxa. Only the interval in which the preservation allowed for quantitative analysis is shown here.

5. Discussion

5.1 Environmental reconstruction

5.1.1 Marine environment

The irregular palynological records and evidence of disconformities and major hiatuses show that the Late Triassic in Svalbard was a time of large-scale sea-level changes, inducing breaks in sedimentation (Vigran et al., 2014). Low subsidence rates resulted in limited accommodation space and low sedimentation rates during the deposition of the Wilhelmøya Subgroup in Spitsbergen (Johannessen & Embry, 1989; Rismyhr et al., 2018). The Barents Shelf most likely had a very low depositional gradient during the Late Triassic-Middle Jurassic (Rismyhr et al., 2018), making the region highly sensitive to relative sea-level fluctuations.

The De Geerdalen Formation was deposited as a delta system prograding from the southeast (Klausen et al., 2015; Rød et al., 2014). The siltstones at the top of the De Geerdalen Formation indicate shallow shelf to delta-plain environments (Lord et al., 2017). The Knorringfjellet Formation of the Wilhelmøya Subgroup disconformably overlies the De Geerdalen Formation (Mørk et al.,

1999; Nagy & Berge, 2008; Vigran et al., 2014). This erosional surface indicates a fall in relative sea level, allowing river systems to extend wide and far out onto the subaerially exposed low gradient shelf, which resulted in an unconformity with limited erosional relief (Rismyhr et al., 2018).

The lower part of the Knorringfjellet Formation shows a fining upwards transgressive trend starting at the base of the Slottet Bed, indicating a period of sea level rise (Nagy & Berge, 2008; Rismyhr et al., 2018). The presence of phosphate seen in thin sections throughout the lower interval of the Knorringfjellet Formation indicates general suboxic conditions around the sediment-water interface (Arning et al., 2009). Phosphate rich sediments are formed by phosphogenesis; the process of apatite precipitation. Phosphogenesis is generally thought to take place in suboxic sediments close to the sediment-water interface, with episodic anoxia and steep or dynamic redox gradient conditions (Arning et al., 2009; Hiatt et al., 2015). It is associated with a specific bacterial metabolic process; polyphosphate utilization by sulfide-oxidizing bacteria results in the rapid precipitation of apatite (Crosby & Bailey, 2012). Micropaleontological evidence has also indicated restricted environmental conditions during the deposition of the formation, with hyposaline waters and hypoxia in near bottom waters (Nagy & Berge, 2008). The rise in relative sea level during the deposition of the Slottet Bed would have led to rapid landward migration of the low-gradient shoreline, trapping sediments within the coastal zone. Therefore, more distal parts of the shelf would become starved of clastic sediment, increasing the susceptibility for the precipitation of authigenic phosphate minerals (Rismyhr et al., 2018).

Observations of thin sections of the Slotted Bed indicate there was at least one phase of phosphatic coated grain formation at the bottom of the bed, and likely another phase in the middle of the bed. The origin of deposits with phosphatic coated grains remains incompletely understood, however it is widely accepted that direct precipitation of phosphate occurs near the sediment-water interface and requires distinct environmental conditions (Arning et al., 2009; Crosby & Bailey, 2012; Hiatt et al., 2015; Pufahl & Grimm, 2003). Arning et al. (2009) and Pufahl and Grimm (2003) propose that phosphatic coated grains are formed in the upper 5-20 cm of sediment, in organic-rich sediments under suboxic to anoxic conditions (figure 7). Here, phosphatic coated grains are most likely formed by repeated reworking caused by high turbulence, with episodically fluctuating redox conditions playing a crucial role (Arning et al., 2009). The development of phosphatic coated grains in the Slotted Bed therefore indicates disturbed, unstable environments with episodes of severe anoxia. The fragmented nature of the coated grains found in the middle of the Slottet Bed, especially sample FT23/10 at 2.9 m height, suggests a higher degree of reworking in this interval. In the samples in the middle of the Slottet Bed, in particular in sample FT23/11 at 3.05 m height, the phosphate grains are partly pyritized. Abundant pyrite can be formed secondarily during phases of enhanced organic matter supply, still very early after the formation of the phosphatic laminae (figure 7B; Arning et al., 2009). This indicates there might have been several periods of enhanced organic matter supply resulting in pyritization of the coated grains found in the middle of the Slottet Bed.

The phosphatic coated grains observed in this study show similarities with the coated grains displayed by Larina et al. (2019) and Arning et al. (2009). In the coated grains of the Slottet Bed the quartz nuclei are usually larger, while the phosphatic coating is developed on average a bit thinner. The alternating darker and lighter brown phosphate laminae are very similar in colour to the concentric laminae in the grains displayed by Larina et al. (2019) and Arning et al. (2009). Compared to the phosphorite deposits of Larina et al. (2019) and Arning et al. (2009) the coated grains are clearly less abundant in the Slottet Bed sediments. For the coated grains observed by Larina et al. (2019), it was suggested the anoxic conditions that allowed for coated grain formation might have been the result of intensified oceanic upwelling and OMZ expansion. A similar process could have taken place during the deposition of the Slottet Bed. Palynological analysis showed dinocysts and

palynoflora were poorly preserved in the depositional environment of the Slottet Bed, likely because the small-sized palynomorphs were washed out with the fine-grained sediments.

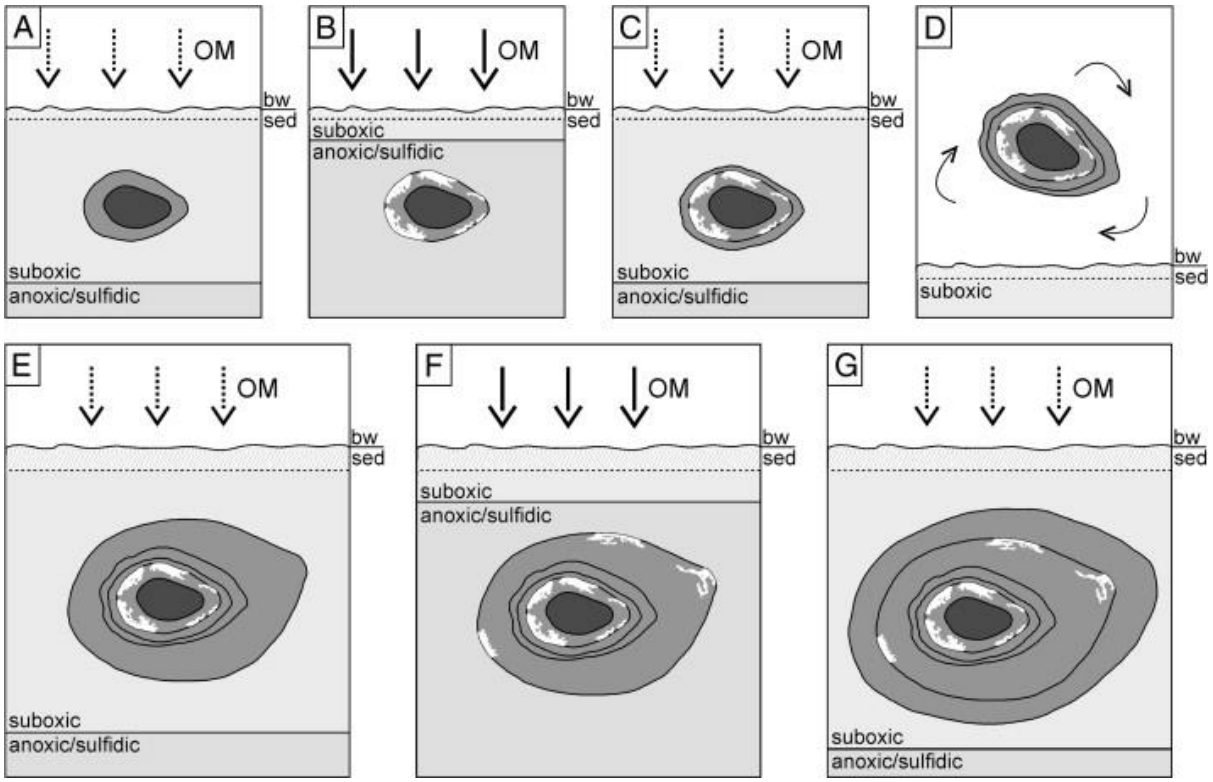

Figure 7: Scenario of phosphatic coated grain formation proposed by Arning et al. (2009). (A) Apatite layers are formed in the suboxic zone close to the bottom water (bw)/sediment (sed) interface. Organic matter (OM) accumulated from the water column and was degraded. (B) During times of enhanced organic matter supply, the anoxic/sulfidic zone moved upwards. Hydrogen sulfide induced pyrite formation in the outer apatite layer. (C) A decreasing organic matter supply, and thus, a downward moving anoxic/sulfidic zone led to the formation of the next apatite layer. (D) Coated grains were eroded, transported, and the outer apatite layer was partially abraded and corroded. (E) After the return to a lower energy regime and coated grain redeposition, apatite precipitation around coated grains was reinitiated under the same conditions as in (A). (F) A new episode of increasing organic matter supply caused repeated pyrite formation. (G) Formation of the outermost apatite layer under conditions as in (A) (Arning et al., 2009).

The fining upwards development of the lower part of the Knorringfjellet Formation suggests upward-deepening and potentially an upwards decrease in sedimentation rates. The transgressive depositional sequence continues up until a glauconitic deposit, where Rismyhr et al. (2018) place a Maximum Flooding Surface (MFS; figure 8), marking a transition to a regression. The lower palynological zone of the Knorringfjellet Formation is dominated by dinocyst species, in particular *Rhaetogonyaulax* spp., *Heibergella* spp. and *Sverdrupiella* spp. The dinoflagellate cyst assemblage recognized in this study shows similarities with a Norian assemblage from the Sverdrup Basin, Arctic Canada, described by Bujak and Fisher (1976). The genera *Sverdrupiella*, *Heibergella*, *Noricysta*, and *Hebecysta* are both recognized in Arctic Canada and at Festningen. However, *Sverdrupiella* spp. are by far the most dominant in the Sverdrup Basin and *Rhaetogonyaulax* sp. was barely observed there, in contrast to the dominance of *Rhaetogonyaulax* spp. at Festningen. Fisher and van Helden (1979)

did report abundant *Rhaetogonyaulax* spp. in Arctic Canada and proposed these were new species, as the encountered specimen consistently differed from *R. rhaetica* reported from Europe. Most *Rhaetogonyaulax* spp. specimens recognized in this study show a stronger similarity to specimens of Fisher and van Helden (1979), especially *R. tortuosa*. Some specimens are more similar to *R. rhaetica* specimens reported from Europe (i.e. Lindström et al., 2023), however. The poor preservation did not allow for classification on the species level for most encountered specimen. As Vigran et al. (2014) have suggested, the similarities between the assemblages from Svalbard and Arctic Canada may reflect an Arctic circumpolar correlative event during the Norian. The presence of phosphate and the micropaleontological evidence of Nagy and Berge (2008) indicate persisting hyposaline waters and less severe low oxygen conditions in this interval.

The interval overlying the MFS consists of an alternation of deeper marine shale intervals and more shallow siderite cemented sandstone beds (Nagy & Berge, 2008; Vigran et al., 2014). This indicates multiple cycles of relative sea level fall and rise, with possible sedimentary breaks occurring at the siderite cemented beds. *Rhaetogonyaulax* spp., *Sverdrupiella* spp. and *Heibergella* spp. abundances decreased after a period of sea level fall and subsequent rise, as indicated by the preceding siderite cemented sandstone bed. Similarly, dinocyst taxa almost disappear after a siderite cemented shallow water deposition.

5.1.2. Terrestrial environment

Palynological analysis of the Festningen section revealed diverse assemblages, which can be used to reconstruct the terrestrial environment. While the poor preservation at the top of the De Geerdalen Formation and in the Slottet Bed did not allow for a vegetational reconstruction, an ecological reconstruction can be made for the *Rhaetogonyaulax* and *Cerebropollenites* zones.

The identified fern, cycad/ginkgo, seed fern, moss and clubmoss taxa are all linked to lowland and mire environments (table 1). These parent groups cover by far the largest part of the assemblage (figure 6), therefore lowland mires were likely the most dominant landscape around the Festningen area during this time period. While mostly the cycads/ginkgos and some seed ferns would have occupied the canopy in these lowland areas, ferns dominated the understory and the ground cover, together with mosses and clubmosses.

Conifer taxa are generally found in more upland, well-drained coastal areas and prefer drier climates (table 1). Conifers are the third most abundant major plant group, however relative abundances do not exceed more than 10% of the total assemblage (figure 6). In areas with higher elevation and better drainage mire vegetation would have more difficulty adapting, allowing conifers to dominate the canopy and understory of these environments. The peak in abundance of conifers in the lower part of the *Cerebropollenites* zone might indicate there was an expansion of drier environments during this time period. *Deltoidospora spp.*, *Concavisporites spp.* and *Monosulcites spp.* are thought to prefer drier patches in mire/lowland environments (table 1). Similar to conifers, these taxa peak in the lower part of the *Cerebropollenites* zone, with combined around 20% of the terrestrial assemblage, compared to 14% in the *Rhaetogonyaulax* zone and 12% in the upper part of the *Cerebropollenites* zone. This might further suggest a relatively drier environment during the deposition of this interval and a return to wetter environments in the upper part of the *Cerebropollenites* zone.

Research from Greenland has shown there is a disconnect between macrofossil and sporomorph records during the Triassic-Jurassic, which can be explained by underrepresentation of certain plant groups in the sporomorph record (Mander et al., 2010). Monosulcate pollen grains are shown to be underrepresented in the palynological record compared to the macrofossil abundance

(Mander et al., 2010). This pattern extends to Mesozoic sediments worldwide (Frederiksen, 1980). Therefore, cycads/ginkgos might be an even more dominant plant group than the relative abundances suggest, although the abundance of monosulcate pollen in the Festningen section is already relatively high compared to assemblages from Greenland (Mander et al., 2013) and Europe (i.e. Bos et al., 2023).

5.2. Biostratigraphic age interpretations and correlations

The deposits of the Wilhelmøya Subgroup in Svalbard are generally thought to record Norian to Early Jurassic ages (Dypvik et al., 1985; Paterson & Mangerud, 2015; Rismyhr et al., 2018; Smelror et al., 2019; Vigran et al., 2014). In early papers describing the palynology of the Wilhelmøya Subgroup a Rhaetian age was assigned to the lower part of the formation based on comparison with Northwestern Europe (Bjærke & Dypvik, 1977; Bjærke & Manum, 1977; Smith, 1975; Smith et al., 1975). Fisher (1979) showed that these characteristic 'Rhaetian' assemblages extend down into the Norian by independently dating subsurface sections in Arctic Canada. A Norian age for the lower part of the Wilhelmøya Subgroup is supported by the presence of bivalves and Sirenitid ammonoids assigned to the Kerri ammonoid Zone on Hopen, southeast Svalbard (Korčinskaja, 1980; Smith, 1982).

The palynology of the Wilhelmøya Subgroup at the Festningen section specifically has been analysed by Vigran et al. (2014) and Rismyhr et al. (2018). The top of the Isfjorden Member has been dated to Carnian/Norian by Vigran et al. (2014) and Late Carnian by Rismyhr et al. (2018). This is supported by geomagnetic polarity data on Hopen, placing the top of the De Geerdalen Formation within the Carnian and the Slottet Bed around the Carnian-Norian boundary (Lord et al., 2014). The poor preservation of the palynomorphs in the samples of this interval did not allow for any new insights in this part of the biostratigraphy. The interval was named *Protodiploxipinus* zone following Paterson and Mangerud (2015) and Rismyhr et al. (2018), therefore a similar Late Carnian age is assumed.

Both Vigran et al. (2014) and Rismyhr et al. (2018) dated the lower part of the Knorringfjellet Formation to an early to middle Norian age based on the abundance of the dinocyst taxa *Rhaetogonyaulax* spp., *Sverdrupiella* spp. and *Heibergella* spp., which are associated with the Norian. The Norian age of this assemblage is corroborated by the macrofossil evidence on Hopen (Korčinskaja, 1980; Smith, 1982). This study shows these taxa are dominant up to 7 m height in the Festningen section. The *Rhaetogonyaulax* spp. zone of this study is therefore similarly interpreted to be of Norian age. Above 7 m height the dominance of the Norian dinocyst species ceases, however. This is where the biostratigraphic interpretations of the Festningen section start to diverge (figure 8).

Vigran et al. (2014) suggest that the presence of the dinocyst taxon *Cleistosphaeridium* sp. and the pollen species *Cerebropollenites thiergartii*, starting around 5 m above the base of the Wilhelmøya Subgroup, are evidence for a Jurassic age. Because of this, the boundary from the Tverrbekken Member to the Teistberget Member is placed here by Vigran et al. (2014). Although species thought to be of a Jurassic age occur, the assemblages are still dominated by Triassic palynomorphs, Vigran et al. (2014) explain this by suggesting the Triassic taxa are reworked. No abundancies of the Triassic taxa interpreted as reworked were indicated by Vigran et al. (2014).

Rismyhr et al. (2018) analysed the sedimentology and stratigraphy of the Wilhelmøya Subgroup in four drill cores from Longyearbyen CO_2 Lab wells and conducted complementary studies at two outcrops including Festningen, which is located 40–45 km west of the drill sites. 33 samples were analysed for palynology from two different drill cores, however only one sample from the lower part of the Wilhelmøya Subgroup in the Festningen section was examined. Instead of a

subdivision into the Tverrbekken and Teistberget Members Rismyhr et al. (2018) subdivides the Wilhelmøya Subgroup in 3 sequences separated by lithologically and/or biostratigraphically well-defined disconformities. The first sequence records deposition in the Early Norian, the second sequence in the Early-Middle Toarcian and the third sequence in the Late Toarcian-Aalenian. It is argued by Rismyhr et al. (2018) that at Festningen the complete Wilhelmøya Subgroup/Knorringfjellet Formation consist of the Early Norian sequence 1, with sequence 2 being absent and sequence 3 being only thinly developed as the Brentskardhaugen Bed at the top of the subgroup. Rismyhr et al. (2018) state the reports of *Cleistosphaeridium* sp. and *C. thiergartii* by Vigran et al. (2014) are unconvincing as Jurassic markers, considering the assemblage is still dominated by characteristic Late Triassic taxa. However, no new samples were analysed in the top interval of the formation.

This study recognized mostly Triassic marker species and did not identify *Cleistosphaeridium* sp. in the upper part of the formation. However, *C. thiergartii* was observed in most samples in this interval. Based on these results and earlier available research, three possible interpretations for the age of the *Cerebropollenites* zone can be proposed: 1) The interval was deposited in the Early Jurassic and therefore all Triassic marker species are reworked. 2) The complete Knorringfjellet Formation in the Festningen section is of a Norian age. This would imply the identified *C. thiergartii* is actually a different species with a similar appearance; or *C. thiergartii* originates a lot earlier than previously reported. 3) The upper interval records Rhaetian deposits. In this scenario, *C. thiergartii* occurs earlier than commonly reported and the Triassic marker species are not reworked.

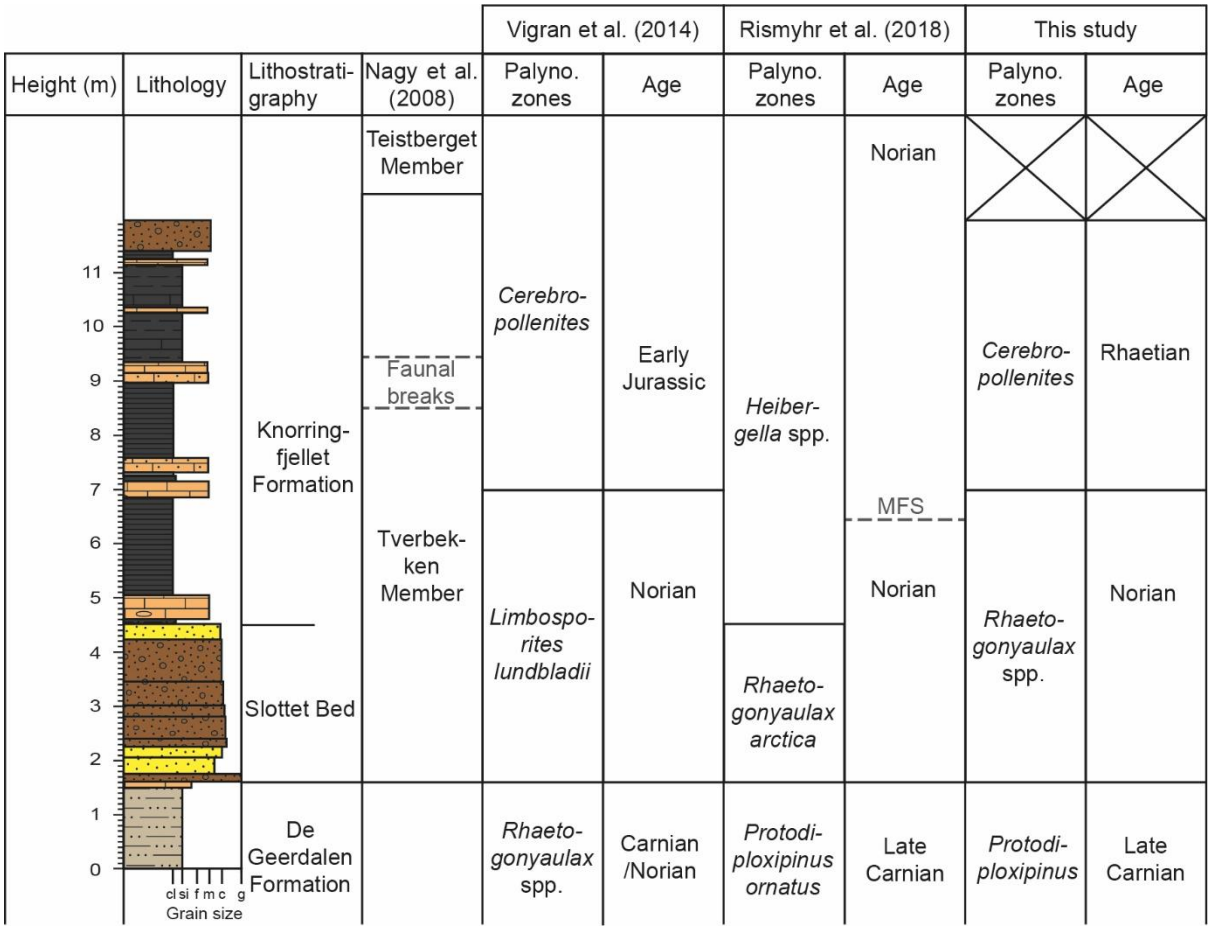

Figure 8: Comparison of biostratigraphic frameworks of earlier studies and a new interpretation from this study.

5.2.1 Early Jurassic age with reworked Triassic taxa

Considering the dominance and diversity of the Triassic marker taxa recognized in the *Cerebropollenites* zone, an Early Jurassic age might not be the most likely interpretation. As the preservation is poor in most samples, no real argument for large scale reworking in this interval can be made based on the appearance of the specimens. There is also no increase in the amount of poorly preserved indeterminable pollen or spores in the *Cerebropollenites* zone, compared to the *Rhaetogonyaulax* spp. zone.

The Triassic spore taxa *Kyrtomisporis* spp., *Aratrisporites* spp. and *Zebrasporites laevigatus* are found more commonly in the interval where they would be reworked than in the Norian interval below. Other Triassic marker taxa do not show a decline in abundance at the zone boundary, and *Semiretisporis* sp. was only identified in the *Cerebropollenites* zone. On top of that, even more Triassic marker species, which were not recognized convincingly in this study, were reported by Vigran et al. (2014): *Camarozonosporites* spp., *Limbosporites lundbladii* and *Rogalskaisporites barentzii*. The sharp decrease in abundance of *Rhaetogonyaulax* spp., *Sverdrupiella spp.* and *Heibergella* spp. might indicate these dinocyst taxa are reworked in the upper interval. This might be the case especially for *Rhaetogonyaulax* spp., as specimen in the upper interval were often fragmented and less clearly defined. *Noricysta* spp. and *Hebecysta* sp., dinocysts also associated with the Triassic, increase in abundance at the start of the *Cerebropollenites* zone, however. In addition,

Veryhachium spp. abundance peaks in the top 2 m of the section, while according to Rismyhr et al. (2018) this acritarch has never been described as a dominating element in Lower Jurassic deposits in the region. Vigran et al. (2014) used *Cleistosphaeridium* sp. as a marker for the Early Jurassic. Rismyhr et al. (2018) argue against this by stating this taxa was never previously used as a marker for the Early Jurassic. *Cleistosphaeridium sp.* was also not even recognized in this study, leaving *C. thiergartii* as the only possible marker for the Jurassic.

Besides that it seems unlikely all Triassic taxa in the *Cerebropollenites* zone are reworked, the absence of any other characteristic Early Jurassic taxa furthermore suggests that the interval is still of Triassic age. Taxa of the Early Jurassic composite assemblage zone from Rismyhr et al. (2018) are not present in the *Cerebropollenites* zone at Festningen. Zircon age data of Bue and Andresen (2013) does suggest mixing in of older Triassic sediments occurred in the Early Jurassic in Svalbard. In Early Jurassic sediments like this a more mixed assemblage with several Jurassic taxa would be expected, however, and not an assemblage completely dominated by Triassic palynomorphs. According to personal communication by T. Bjærke the top of the Wilhelmøya Subgroup at Festningen contains Rhaetian palynomorphs (Bäckström & Nagy, 1985), which would also contradict the Jurassic interpretation of Vigran et al. (2014).

A foraminiferal succession of the Knorringfjellet Formation in Festningen presented by Nagy and Berge (2008) seems to provide additional evidence against the Jurassic interpretation of Vigran et al. (2014). A foraminiferal similarity index reveals no faunal break can be recognized at the transition to the *Cerebropollenites* zone. If the transition to the *Cerebropollenites* zone is a Triassic-Jurassic boundary, one would expect major faunal breaks there. In contrast, faunal breaks are recognized around 9 m height in the section (Nagy and Berge, 2008; figure 8), around the transition where dinocysts almost disappear. They place the transition of the Tverrbekken Member to the Teistberget Member even higher in the section, at ~11.8 m above the base of the formation, at a heavily bioturbated and partly siderite cemented top surface of a sandstone.

Dypvik et al. (1985) concluded a Wilhelmøya Subgroup section in Bohemanflya (north of Isfjorden, central Spitsbergen) may be of a Norian or Rhaetian age. Here, the Brentskardhaugen Bed rests unconformably on Upper Triassic deposits. It is suggested that the sequence at this section represents a marginal development of the lower part of the Wilhelmøya Formation. Unpublished palynological data seem to demonstrate a correlation between the Wilhelmøya Subgroup assemblages at Bohemanflya and Festningen (Dypvik et al., 1985). The Festningen section might therefore represent a similar marginal development of the Wilhelmøya Subgroup. Another similar interpretation of a Wilhelmøya Subgroup sequence without Jurassic deposits was made at the section of Syltoppen by Rismyhr et al. (2018).

5.2.2 *Cerebropollenites thiergartii* as a stratigraphic marker

Cerebropollenites thiergartii and related taxa have been re-evaluated by Gravendyck et al. (2023). A recombination of the genera *Cerebropollenites* and *Sciadopityspollenites* as *Sciadopityspollenites* was proposed. Most literature relevant for this study has used the term *Cerebropollenites*, however. Therefore, this study continues using *Cerebropollenites* and uses *Sciadopityspollenites* as a synonym when referring to photomicrographs from Gravendyck et al. (2023).

C. thiergartii has often been suggested as a palynological marker for the base of the Jurassic (Fisher & Dunay, 1981; Kürschner et al., 2007; Mander et al., 2010; von Hillebrandt et al., 2007; von Hillebrandt et al., 2013). It usually occurs around the turn to more negative $\delta^{13}C$ values in the lower part of the initial/Spelae CIE, above the extinction level of Triassic biota but significantly below the first occurrence of Jurassic ammonites (von Hillebrandt et al., 2013). *C. thiergartii* has also been reported to first occur around the Triassic-Jurassic boundary in high latitudes; in Greenland (Mander

et al., 2010, 2013; Pedersen & Lund, 1980), in the Sverdrup Basin in Arctic Canada (Embry & Suneby, 1994; Suneby & Hills, 1988) and in the eastern Svalbard island Kongsøya (Kong Karls Land island group) (Smelror et al., 2019). Mander et al. (2010) interpreted the incoming of *Cerebropollenites* spp. in an assemblage from East Greenland to be of latest Rhaetian age. Smelror et al. (2019) used the earliest appearance of *C. thiergartii* as an indication the Hettangian age starts at that level.

Some occurrences of *C. thiergartii* before the Jurassic have been reported as well. *C. thiergartii* has been documented in the latest Rhaetian in sections in Austria (Bonis et al., 2009), De Jersey (1971) reported *C. thiergartii* from Upper Triassic sediments in Australia and Morbey (1978) reported *C. thiergartii* starting from the Late Rhaetian in northwestern Europe. Lund (1977) documented *C. thiergartii* as early as the Middle Rhaetian in two cored wells (Rødby 1 and Maasbüll 1) situated on the northern flank of the Northwest German Basin. Lund (1977) does note, however, that early members of *C. thiergartii* can be difficult to separate from other taxa. Particularly *Chasmatosporites apertus* specimens with an uneven tectum can be difficult to distinguish from *C. thiergartii* and this distinction was less clear in the Middle Rhaetian. Gravendyck et al. (2023) question the findings of Lund (1977) and suggest the specimen depicted as *C. thiergartii* by Lund (1977) is better assigned to the epithet *macroverrucosus*, as it does not show the typical morphological features of *C. thiergartii*. Although *C. macroverrucosus* possesses rugulae and *C. thiergartii* verrucae, distinguishing *C. thiergartii* from *C. macroverrucosus* specimens with relatively small and densely packed sculptural elements can be difficult from photographs, especially when preservation is poor like in many samples of this age (Gravendyck et al., 2023).

Lindström, van de Schootbrugge, et al. (2017) suggest *C. thiergartii* might not be a reliable marker for the Triassic-Jurassic boundary, as its first occurrence varies between different localities. It can also be quite difficult to recognize and is often very rare when it first appears in the stratigraphical record. The discrepancies in first occurrences of *C. thiergartii* may also be an effect of the substantial sea-level changes associated with the T-J transition; the regression-transgression couplet (Lindström, van de Schootbrugge, et al., 2017). Evidence of extensive sea-level fall quickly followed by sea-level rise is found widely across Europe at the Triassic-Jurassic boundary. This regression and transgression resulted in highly condensed or partially missing strata in many sections (Hallam & Wignall, 1999).

The 2nd and 3rd possible age interpretations of the *Cerebropollenites* zone are in agreement on its Triassic nature, arguments for a Norian or Rhaetian interpretation depend mostly on how reliable the observed *C. thiergartii* is deemed as a stratigraphic marker. Both *C. thiergartii* and *C. macroverrucosus* have never been recognized in the Norian or in the early Rhaetian, it therefore seems unlikely an interval with *C. thiergartii* is of a Norian age. For the Norian age interpretation the apparent occurrence of *C. thiergartii* could be explained by an incorrect identification. Rismyhr et al. (2018) argue *Cerebropollenites thiergartii* was only observed rarely in two samples by Vigran et al (2014), implying these specimens could have been wrongly identified. In this study *C. thiergartii* is found consistently in most samples above 8 m height in the section, however. *C. thiergartii* is often rare when it first appears in the stratigraphic record (Lindström, van de Schootbrugge, et al., 2017), the low abundance at the Festningen section is therefore in line with what would be expected for early occurrences of this species.

Possible species that could be difficult to separate from *C. thiergartii* include: *Chasmatosporites* (*apertus*) specimens with an irregular tectum (figure 9 D.9 & D.10), *Cerebropollenites/Sciadopityspollenites macroverrucosus* specimens with relatively small and densely packed sculptural elements (figure 9 D.6) and *Protodiploxipinus ornatus* or *decus* specimens without visible sacci (figure 9 D.7). In figure 9 encountered specimen counted as *C. thiergartii* and other specimen showing some resemblance to *C. thiergartii* are compared to specimen presented in previous studies. Some specimens that were first noted as possibly being *C. thiergartii* were later

counted as *Chasmatosporites* spp. or *Protodiploxipinus* spp. (figure 9 B and C). Specimens that were ultimately counted as *C. thiergartii* do not show a strong resemblance to *Chasmatosporites apertus* and *Protodiploxipinus ornatus* or *decus* specimens. Comparing the counted specimens to pictures of *Cerebropollenites/Sciadopityspollenites thiergartii* and *macroverrucosus* the encountered specimens show a stronger similarity to the epithet *thiergartii*; containing verrucae instead of rugulae (figure 9 D).

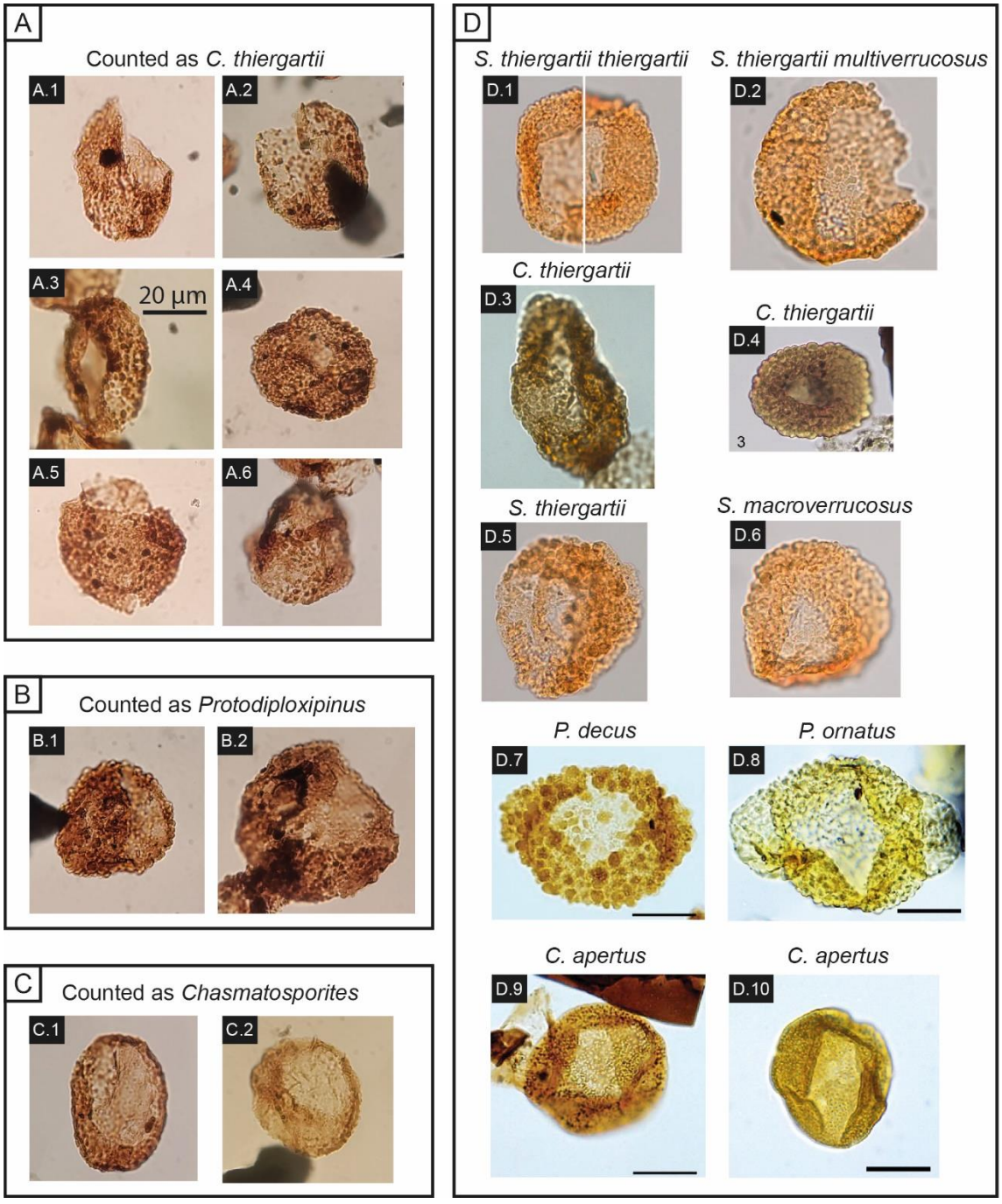

Figure 9: Comparison of specimen resembling Cerebropollenites thiergartii encountered in this study ***(A-C)*** *and photomicrographs of several related species from literature* ***(D)****. All pictures are to the same scale.* ***(A1-6)*** *Specimens from this study that were counted as Cerebropollenites thiergartii;* ***(B1-2)*** *Encountered specimens that were counted as Protodiploxipinus spp.;* ***(C1-2)*** *Encountered*

specimens that were counted as Chasmatosporites spp.; ***(D1)*** *Sciadopityspollenites thiergartii thiergartii, new subspecies as defined by Gravendyck et al. (2023);* ***(D2)*** *Sciadopityspollenites thiergartii multiverrucosus, new subspecies as defined by Gravendyck et al. (2023);* ***(D3)*** *Cerebropollenites thiergartii (Mander et al., 2013);* ***(D4)*** *Cerebropollenites thiergartii (Lindström, Erlström, et al., 2017);* ***(D5)*** *Specimen tentatively assigned to Sciadopityspollenites thiergartii but showing transitionary ornamentation to S. macroverrucosus (Gravendyck et al., 2023);* ***(D6****) Densely regulate form of Sciadopityspollenites macroverrucosus (Gravendyck et al., 2023);* ***(D7)*** *Protodiploxipinus decus (Paterson et al., 2019);* ***(D8)*** *Protodiploxipinus ornatus (Paterson & Mangerud, 2017);* ***(D9)*** *Chasmatosporites apertus (Paterson et al., 2019);* ***(D10)*** *Chasmatosporites apertus (Paterson & Mangerud, 2017).*

Most depicted specimens of the epithet *thiergartii* do seem to be slightly larger (~50 µm) than specimens encountered in this study (35-40 µm), with the exception of the specimen in Lindström, Erlström, et al. (2017). The specimens in this study are not really suitable to be assigned decisively to one of the subspecies defined by Gravendyck et al. (2023) (*thiergartii* or *multiverrucosus*). The depiction of subspecies *multiverrucosus* does seem larger-sized and with coarser ornamentation, therefore specimens of this study might be closer to the subspecies *thiergartii*, with a finer ornamentation.

Based on these comparisons, it can be concluded that the *C. thiergartii* specimens encountered in this study most closely resemble earlier depictions of *C. thiergartii* and do not seem to be wrongly identified. If the complete section of the Knorringfjellet Formation is of a Norian age, this would mean *C. thiergartii*, or at least a species very closely resembling *C. thiergartii*, occurred millions of years earlier than ever reported. Even if the *Cerebropollenites* specimens actually belong to the epithet *macroverrucosus*, this would still be a marker species that was never found in the Norian. Therefore, a Rhaetian age seems to be the most likely explanation for the occurrence of *C. thiergartii* together with Triassic marker species. Accordingly, this study proposes a Rhaetian age for the *Cerebropollenites* zone.

The biostratigraphic results of this study cast further doubt on the reliability of *C. thiergartii* as a marker for the Triassic-Jurassic boundary. The first occurrences of *C. thiergartii* appear to vary strongly between different localities. Similar to the Festningen section, a core section by Vigran et al. (2014) in the Nordkapp Basin in northern Norway (CORE 7230/5-U-3) is most likely wrongly interpreted as Early Jurassic. The assemblage here contains overwhelming evidence for a Rhaetian age that was all interpreted as reworked (including: *Riccisporites tuberculatus*, *Protodiploxipinu*s spp., *Ovalipollis pseudoalatus*, *Lunatisporites* spp, *Triadispora* spp., *Quadraeculina anellaeformis, Limbosporites lundbladii*, *Rogalskaporites barentzii*, *Kyrtomisporis* spp., *Semiretisporis gothae*, *Cingulizonates rhaeticus* and *Aratrisporite*s spp.), and only *C. thiergartii* and *C. macroverrucosus* are used as Jurassic indicators. In some cores from the Hammerfest Basin in Norway presented by Vigran et al. (2014) Triassic palynomorphs occurring together with *Cerebropollenites* were interpreted to be reworked as well, however the presence of Triassic marker species is not as overwhelming here.

Hochuli and Vigran (2010) have recorded *Cerebropollenites spp.* in Upper Triassic ditch cutting samples. Vigran et al. (2014) also reported *C. macroverrucosus* and *C. thiergartii* specimens in an interval they interpreted as Rhaetian from a core in the Hammerfest Basin in northern Norway (WELL 7120/12-3). The *Cerebropollenites* specimens were mostly found in cutting samples, and as cutting samples are sometimes contaminated by caved material during the drilling operations (Lindström, 2020), these specimens were interpreted as Jurassic species caved into this Rhaetian interval by Vigran et al. (2014). Now we know *Cerebropollenites* can be found in Triassic assemblages, it should be considered these specimen were wrongly interpreted as caved in. The

'caved in' specimens were mostly found in the upper part of the Rhaetian interval, which could be in agreement with earlier reports of *Cerebropollenites* late in the Rhaetian. There might be more instances worldwide of wrongly interpreted Triassic-Jurassic boundaries based on first low abundance occurrences of *C. thiergartii*. These apparent early occurrences in Svalbard and northern Norway suggest *C. thiergartii* might have originated in high-latitude regions and later migrated to lower latitudes, where it is mostly found close to the Triassic-Jurassic boundary.

5.2.3 Comparison with other Rhaetian assemblages (in Svalbard)

In assemblages interpreted as Rhaetian from the Barents Sea and Hopen *Limbosporites lundbladii* and *Quadraeculina anellaeformis* have been reported as important marker species (Paterson & Mangerud, 2015; Vigran et al., 2014). These species were not found to be a significant part of the assemblage in this study, with only a few questionable finds. *L. lundbladii* and *Q. anellaeformis* were both reported in the *Cerebropollenites* zone by Vigran et al. (2014), however. Therefore, these species probably do occur in this interval, but are hard to be recognized and less abundant than in other areas.

Common occurrences of *Ricciisporites tuberculatus* are often reported in late Rhaetian intervals from the Barents Sea and Greenland (Hochuli & Vigran, 2010; Pedersen & Lund, 1980; Vigran et al., 2014). *R. tuberculatus* was not found in the Festningen section, which might indicate the studied section does not record the late Rhaetian. Vigran et al. (2014) report *Ricciisporites* spp. at Festningen, but not *tuberculatus* specifically. *R. tuberculatus* was reported at a low abundance in the Rhaetian interval studied by Paterson and Mangerud (2015), however, indicating a high abundance is not found everywhere. Absence of common *R. tuberculatus* might therefore not be strong evidence against a late Rhaetian age.

Paterson and Mangerud (2015) defined their possible late Rhaetian interval based on the first occurrence of *Rogalskaisporites ambientis*, although it is found at very low abundances. This species was not identified in this study, Vigran et al. (2014) did report *Rogalskaisporites barentzii* in the *Cerebropollenites* zone at Festningen, however. The epithet *barentzii* seems to be their equivalent of *ambientis*, as no *ambientis* was reported at any section by Vigran et al. (2014) and the plate examples look identical. Similar to *L. lundbladii* and *Q. anellaeformis* this species might therefore be very rare and poorly preserved at Festningen.

In conclusion, the assemblage of the *Cerebropollenites* zone at Festningen shows quite some different marker species abundances compared to other Rhaetian assemblages from Svalbard. Most of these marker species are found at a lower abundance at Festningen, probably due to regional differences and poor preservation. Therefore, these differences do not strongly evidence against a Rhaetian age, although absence of *R. tuberculatus* could indicate a late Rhaetian age is less likely. There seem to be strong regional differences across Svalbard, as large differences in marker species abundances are found between earlier reported assemblages as well (Paterson & Mangerud, 2015; Vigran et al., 2014). Variable precipitation and locally variable groundwater levels over Svalbard might have controlled the regional composition of the flora (Vigran et al., 2014).

The pollen genus *Classopollis* is not found in the samples, in contrast to high abundances in European Rhaetian assemblages (i.e. Lindström, 2021). In Greenland the amount of *Classopollis* is also very low (Mander et al., 2013). *Classopollis* pollen have been shown to decrease in abundance with increasing palaeolatitude (Vakhrameev, 1981), indicating these conifers were probably poorly adapted to the environment of Svalbard.

5.2.4 Unexposed interval of the Knorringfjellet Formation

The top interval of the Knorringfjellet Formation could not be analysed in this study, as it was covered by a thick layer of snow during the sampling. Using the results of Vigran et al. (2014) a new interpretation can be made of the biostratigraphy of this interval. Based on the continued occurrence of Triassic marker species interpreted as reworked, it can be assumed the Rhaetian deposits are found up until ~13 m above the base of the formation, ~2.5 m above the interval analysed in this study. Around 14 meters above the base of the formation Vigran et al. (2014) do not report any Triassic marker species, and in the uppermost analysed sample multiple dinocysts characteristic of Middle Jurassic assemblages were found. Therefore, this could be the actual transition to the Jurassic at the Festningen section. Rismyhr et al. (2018) have suggested this last sample must have been contaminated or misplaced, as they think Middle Jurassic dinoflagellate cyst should not be found here. A future study should be able to provide decisive evidence on the age of the top part of the Knorringfjellet Formation by performing palynological analysis on the snow covered interval.

5.3 TOC and $\delta^{13}C_{org}$ correlations

Nagy and Berge (2008) have performed TOC measurements on the Knorringfjellet Formation of the Festningen section at a lower resolution. Only shale samples were analysed, which were found to contain TOC content ranging from 0.9 to 1.6 %. This is very similar to the values of shale samples measured in this study; ranging from 1.0 to 1.5 %. Nagy and Berge (2008) note that the TOC content of the interval analysed in this study is higher than in the top meters of the Knorringfjellet Formation. An analysis of Middle Permian-Early Triassic samples from the Festningen section show lower average TOC values as well, mostly in the range of 0 to 0.7% (Grasby et al., 2016). Nagy and Berge (2008) suggest the relatively higher TOC content could indicate oxygen depletion was more severe during the deposition of the lower interval of the Knorringfjellet Formation. Low oxygen conditions throughout the lower interval of the Knorringfjellet Formation are supported by the presence of phosphate in the thin sections (paragraph 4.2 & 5.1.1.). TOC values are lower at the coarse-grained shallow water deposits of the Knorringfjellet Formation, this might have been the result of washing out of the fine-grained organic material in the high energy coastal environment.

A large negative carbon isotope excursion was found in the Slottet Bed, which is thought to be deposited in the early Norian. No large isotope excursions have been previously identified around the Carnian-Norian boundary or in the Early Norian. A $\delta^{13}C_{org}$ record from a Carnian-Norian boundary section at Williston Lake, Canada, shows relative stability in carbon cycling during this time period. Samples closely around the boundary interval reveal a negative isotope perturbation of 0.5‰, interpreted to be the result of a decline in net primary production (Williford et al., 2007). A $\delta^{13}C$ dataset of Atudorei and Baud (1997) combined with data of Böhm and Gawlick (1997) shows a consistent trend with a gradual rise in $\delta^{13}C$ values from the Lower Carnian to Lower Norian, followed by a decrease in $\delta^{13}C$ values starting with the Upper Lower Norian.

Around the interpreted transition from the Norian to the Rhaetian a small $\delta^{13}C$ excursion of around 1‰ lower than surrounding samples was measured. As Rigo et al. (2020) have shown, negative CIEs around the Norian-Rhaetian Boundary (NRB) are found at both sides of the Pangaean supercontinent in both the Northern and Southern Hemispheres. The negative carbon isotope shift is thought to have been most likely caused by greenhouse gas emissions from a large-scale volcanic event preceding the NRB. However, no LIP dated to this time period has been recognised yet. In general, the recognized CIEs around the NRB show more negative values and a much larger amplitude than found in this study (Rigo et al., 2020), although a section from west Canada shows an

amplitude of only 1.5 ‰ (Ward et al., 2004). The excursion found in this study might represent a NRB CIE, associated with the global carbon cycle perturbation of this time. However, it is uncertain the exact NRB is even recorded in the Festningen section, as there seems to be a discontinuity and hiatus at the transition from Norian to Rhaetian. On top of that, two of the lowest values are found in coarser siderite cemented layers, while the shale and clay samples in between both resulted in higher values. This could indicate local processes are the dominant factor influencing the $\delta^{13}C$ values in this interval. There is certainly not sufficient evidence to state a negative $\delta^{13}C$ excursion at the NRB was recorded in Festningen.

Another negative CIE of ~-1.7‰, with values ranging from -25.2‰ to -26.1‰, has been identified in the Rhaetian interval of this study. The specific age recorded in this CIE interval is difficult to determine. The occurrence of *Cerebropollenites thiergartii* might be evidence for a late Rhaetian age, however the absence of *Ricciisporites tuberculatus* could argue against a late Rhaetian age. No evidence for decreased arborescent conifers and increased ferns could be found, suggesting the CIE predates the end-Triassic extinction interval. The CIE identified in this interval does align with coarser nodular sandstone and siderite samples, however two shale samples show more negative values as well. A more global influence on this CIE could therefore be more likely. The first global carbon cycle disruption of the end of the Triassic is the Marshi/precursor CIE (Ruhl & Kürschner, 2011). This precursor CIE occurs before the extinction interval and is related to the earliest CAMP mafic intrusions (Davies et al., 2017). The top CIE recognized in this study could possibly be correlated to this event; or it could be another more regional carbon cycle perturbation earlier in the Rhaetian. $\delta^{13}C_{org}$ measurements from the Lombardy Basin, northern Italy, covering the entire Rhaetian revealed 7 negative carbon isotope peaks, showing carbon cycle perturbation occurred earlier in the Rhaetian as well (Zaffani et al., 2018). A future study on the snow covered top part of the Knorringfjellet Formation could provide further evidence in support of or against a possible correlation to the precursor CIE.

As the CIEs identified in this study largely correlate with lithology changes, future Mercury measurements on samples of the Knorringfjellet Formation could better assess the extent of volcanic influence. Elevated Hg/TOC values coinciding with the CIEs would reveal volcanic influence, otherwise the $\delta^{13}C$ data of this section probably only reflect local carbon cycle disturbances.

5.4 Environmental change linked to volcanism and climate change

5.4.1 Slottet Bed deposited during global warming

The presence of phosphatic coated grains in late Rhaetian deposits from northeastern Panthalassa are considered to indicate anoxic conditions resulting from intensified oceanic upwelling and oxygen minimum zone expansion (Larina et al., 2019). In this period preceding the ETME there is indication for periods with extreme temperature increase and atmospheric CO_2 rise, potentially caused by early CAMP dike and sill intrusions in organic rich sediments (Davies et al., 2017). Larina et al. (2019) therefore hypothesize that the intensified oceanic upwelling and oxygen minimum zone expansion might have been related to volcanic induced climate warming. Widespread occurrence of phosphatic bonebed deposits in Rhaetian sediments across the European shelves have been interpreted as the lithological signature of climatically driven perturbations of P- and C-cycling as well (Suan et al., 2012). Poorly oxygenated conditions enhancing phosphorus regeneration from sedimentary organic matter into the water column probably provided the main source of phosphate of these beds. The interval showing oxygen depletion and accelerated P-cycling coincides with a negative CIE predating the initial isotope excursion characterizing Triassic-Jurassic boundary strata, indicating the

phosphatic bonebeds similarly might be related to early episodes of CAMP activity (Suan et al., 2012).

Although at Festningen no phosphate rich beds are found in the interval interpreted as Rhaetian, the Norian phosphatic deposits similarly align with a CIE, suggesting a comparable process might be taking place. The Slottet Bed was deposited during a period of sea level rise, which could have been the consequence of global warming. However, no global carbon cycle perturbation, LIP or global warming interval has been recognized for the proposed early Norian age of the Slottet Bed. The early Norian is associated with lower temperatures (Trotter et al., 2015) and a return to arid conditions after the Carnian Pluvial Episode (Simms & Ruffell, 1989). Based on this, it seems more likely the deposition of the Slottet Bed was the result of regional environmental conditions allowing for phosphogenesis and coated grain formation during the early Norian. However, oxygen isotope measurements on conodont assemblages from Canada do indicate two short peaks in Sea Surface Temperature at and just after the Carnian-Norian transition (Sun et al., 2020). If the base of the Slottet Bed was deposited exactly around the Carnian-Norian boundary, which is the preferred dating by Lord et al. (2014), the two phases of coated grain formation might be related to these two temperature peaks.

LIP's and global warming intervals have been described earlier in the Carnian stage and later in the Norian. The Wrangellia LIP, coinciding with multiple negative $\delta^{13}C$ shifts (Dal Corso et al., 2018) and followed by an intense warming period (Trotter et al., 2015), is dated to the mid-Carnian. The Angayucham LIP is estimated at an age of 214 Ma with a standard deviation of 7 Ma. Although the dating has a strong uncertainty, Os isotopes seem to suggest the onset of the Angayucham volcanism is found at the start of the late Norian (Sato et al., 2023). An intense global warming period is also found during the late Norian (Sun et al., 2020; Trotter et al., 2015). The Slottet Bed could be correlated to one of these two volcanic phases with carbon cycle perturbations, however this would mean the dating to the Early Norian is inaccurate.

Multiple studies support a dating to the early Norian for the Slottet Bed. The top of the De Geerdalen Formation is dated to the latest Carnian to earliest Norian based on palynological and magnetostratigraphic studies (Lord et al., 2014; Vigran et al., 2014). A disconformity is found between the De Geerdalen Formation and the Slottet Bed, however based on biostratigraphic data no evidence for a major hiatus has been documented at this disconformity (Paterson & Mangerud, 2015; Vigran et al., 2014), making an early Norian age the most likely. If the disconformity at the bottom of the Slottet Bed actually does represent a major hiatus, the bed might have been deposited later in the Norian, during the onset of the Angayucham LIP. Because of the unprecise dating of the Angayucham LIP this correlation remains a possibility that should be taken into account. The Angayucham LIP in north Alaska was located quite close to Svalbard during Late Triassic times (figure 2), therefore some influence of the volcanic emissions from this province could be expected in the Archipelago. In this scenario, the two phases of coated grain formation might be related to the two negative shifts in the $^{187}Os/^{188}Os$ ratio linked to the Angayucham LIP by Sato et al. (2023). A correlation to the Wrangellia LIP does not seem very likely, as the mid-Carnian is thought to be deposited in the middle of the De Geerdalen Formation (Vigran et al., 2014). A correlation of the Slottet Bed to the temperature peaks around the Carnian-Norian transition described by Sun et al. (2020) remains best in line with the proposed ages of the stratigraphic units.

5.4.2 Palynological trends and climate change

The relative quantitative distribution of spore, pollen and dinocyst taxa may be a response to changing climates through time. In the Norian interval at Festningen dinocyst taxa are very

dominant, while in the *Cerebropollenites* zone, interpreted as Rhaetian in this study, dinocyst abundance is strongly decreased, especially *Rhaetogonyaulax* spp. In contrast, *Rhaetogonyaulax rhaetica* still occurs commonly till the end of the Rhaetian in Europe (Lindström et al., 2023). Temperatures strongly increased during the late Norian, after which cooler conditions were found during the Rhaetian before the end-Triassic extinction interval (Trotter et al., 2015). The colder conditions of the Rhaetian at Svalbard, situated at a higher paleolatitude, might be a reason Rhaetogonyaulax disappeared earlier here than in Europe. No spore spike indicating environmental disturbance or evidence for declining diversity at the transition from Norian to Rhaetian, similar to Rigo et al. (2020), can be found.

Humid events are associated with low $\delta^{18}O$ warming phases in the Late Triassic (Trotter et al., 2015). The colder interval during much of the Rhaetian identified by Trotter et al. (2015) might therefore be a relatively more dry period. This could explain the peak in conifers, preferring well-drained environments and drier climates, and taxa preferring drier mire patches (*Deltoidospora spp.*, *Concavisporites spp.* and *Monosulcites spp.*) in the lower part of the *Cerebropollenites* zone. As temperatures were starting to increase again, there could have been a return to wetter environments, coinciding with the decrease of species preferring drier conditions in the upper part of the *Cerebropollenites* zone.

Dinoflagellate cysts almost disappear above a shallow water siderite cemented sandstone bed around 9 m in the section. Around this interval, Nagy and Berge (2008) also recognized faunal breaks in the foraminiferal succession (figure 8). The dinocyst and foraminifera assemblages therefore seem to indicate an environmental change in the marine realm during this period of sea level fall and subsequent rise. No floral evidence for environmental disturbance can be found in the Rhaetian *Cerebropollenites* zone. No significant increase in fern spores relative to the terrestrial counts can be recognized, and no decrease in arborescent conifers was identified. An increase in acritarch abundance is found in the top interval of the *Cerebropollenites* zone. A bloom of acritarchs is usually observed at the Triassic-Jurassic boundary (van de Schootbrugge et al., 2007), however this is normally found after the spore spike and floral extinction interval. It is likely the latest Rhaetian extinction interval was not recorded in the studied interval. Palynological analysis of the top few meters of the Knorringfjellet Formation could determine if a spore spike can be found there or if no palynological evidence for environmental disturbance during the end-Triassic can be found at Festningen.

6. Conclusions

- A new biostratigraphic age interpretation for the Late-Triassic Festningen section is made based on the presence of palynological marker species. The top of the De Geerdalen Formation is likely of a late Carnian age, and all evidence points to a Norian age for the dinocyst dominated lower interval of the Knorringfjellet Formation at Festningen. However, for the upper interval of the Knorringfjellet Formation at Festningen there are three possible age interpretations: Early Jurassic, Rhaetian or Norian. The species *Cerebropollenites thiergartii*, which has often been suggested as a marker for the base of the Jurassic, is observed here together with Triassic marker species. An Early Jurassic interpretation seems the least likely, based on the dominance of Triassic marker species and absence of any Jurassic indicators besides *C. thiergartii*. The Festningen section seems to represent a marginal development of the Wilhelmøya Subgroup, with no Jurassic deposits or only at the

very top, similar to the Bohemanflya and Syltoppen sections around Isfjorden. A Rhaetian age can best explain the occurrence of *C. thiergartii* together with Triassic marker species, as *C. thiergartii* is occasionally reported in the Rhaetian. A Norian age is only possible if the *C. thiergartii* specimens actually belong to a completely different genus, or if *C. thiergartii* originated millions of years earlier than previously reported. This study therefore proposes a Rhaetian age for the upper interval of the Knorringfjellet Formation.

- The biostratigraphic results of this study cast further doubt on the reliability of *C. thiergartii* as a marker for the base of the Jurassic. Besides the Festningen section, a core section in northern Norway is most likely also wrongly interpreted as Early Jurassic purely based on the occurrence of *Cerebropollenites* specimens in a Triassic assemblage. Furthermore, *Cerebropollenites* specimens in Rhaetian intervals from northern Norway might have been wrongly interpreted as caved in. There could be more instances of incorrect interpretations based on first low abundance occurrences of *C. thiergartii*. *C. thiergartii* might have originated in high-latitude regions and later migrated to lower latitudes. These early *Cerebropollenites* specimens are found at low abundances and are relatively small and show relatively fine ornamentation.

- Phosphatic coated grains observed in thin sections of the Slottet Bed indicate disturbed conditions with episodic anoxia, fluctuating redox conditions and repeated reworking. The anoxic conditions allowing for phosphatic coated grain formation might have been the result of intensified oceanic upwelling and OMZ expansion. This could have been related to (volcanic induced) climate warming, as the Slottet Bed aligns with a CIE and was deposited during a period of sea level rise. A correlation to temperature peaks around the Carnian-Norian boundary seems the most likely, as this is the preferred dating for the deposition of the Slottet Bed. Because of the disconformable character of the base of the Slottet Bed and the highly uncertain mid-late Norian dating of the Angayucham LIP, a correlation to this volcanic event later in the Norian is another possibility.

- A vegetational reconstruction was made for the Knorringfjellet Formation above the Slottet Bed based on known botanical affinities of the quantified taxa. Ferns and cycads/ginkgos are the most dominant plant groups throughout the section, followed by conifers. Lowland mires were likely the most dominant landscape around the Festningen area during the Norian and Rhaetian, as the identified fern, cycad/ginkgo, seed fern, moss and clubmoss taxa are all linked to this environment. While cycads/ginkgos would have occupied the canopy in these lowland areas, ferns dominated the understory, and the ground cover together with (club)mosses. Conifer taxa, covering less than 10% of the total assemblage, probably dominated the canopy and understory of the drier, higher elevated areas. A peak in abundance of taxa preferring drier conditions in the lower part of the Rhaetian interval might indicate an expansion of these drier environments. This drier period could be related to the colder interval identified during much of the Rhaetian, with a return to wetter environments as temperatures were starting to increase again. No spore spikes indicating environmental disturbances were found at the transition from Norian to Rhaetian or in the top of the Rhaetian interval. The end-Triassic extinction interval might not have been recorded at Festningen.

- The dinocyst assemblage dominating the lower interval of the Knorringfjellet Formation shows similarities with Norian assemblages from Arctic Canada, probably reflecting an Arctic circumpolar correlative event during the Norian. A strong decrease in dinocysts coincides

with faunal breaks in the foraminiferal succession, indicating a marine environmental disturbance.

- A negative CIE is recognized at the top of the interval analysed in this study. This CIE could possibly be correlated to the precursor CIE, or it could be another carbon cycle perturbation earlier in the Rhaetian.

Recommendations for further research

- Quantitative palynological analysis should be performed on the top of the Knorringfjellet Formation to obtain decisive evidence for where the Jurassic starts in the Festningen section. Analysis of the top interval can also determine if a spore spike can be found there, or if this cannot be identified in the complete Upper Triassic-Lower Jurassic Festningen section.
- Mercury measurements should be performed on the samples to better assess the intervals with CIEs for volcanic influence. Preferably, Hg, $\delta^{13}C$ and TOC measurements are also performed on samples of the top of the Knorringfjellet Formation not analysed in this study. Based on these additional measurements, it could be decided if the precursor CIE and possibly other Rhaetian CIEs are recorded at Festningen.
- Now we know *C. thiergartii* can occur in Rhaetian deposits, interpretations of a Triassic-Jurassic boundary purely based on the first occurrence of *C. thiergartii* should be re-evaluated, especially for high-latitude regions.

Acknowledgements

This MSc thesis was facilitated by the resources and financing of Utrecht University. I want to thank Natasja Welters and Giovanni Dammers for teaching me the carbon measurement and palynology preparation procedures in the GeoLab. Thanks go out to Desmond Eefting, who performed the $\delta^{13}C$ and TOC measurements for this study, and Leonard Bik, who made thin sections of the rock samples. I want to thank my supervisor Bas van de Schootbrugge for guiding me in the right direction during the research process and for suggesting improvements in my presentation and writing. My second supervisor Remco Bos especially helped me to start up the project and to process my data into clear and visually interesting figures.

Literature

Abbink, O. A. (1998). *Palynological Investigations in the Jurassic of the North Sea Region: Palynologisch Onderzoek in de Jura Van Het Noordzeegebied*. Univ. https://books.google.nl/books?id=hbWTAAAACAAJ

Arning, E. T., Lückge, A., Breuer, C., Gussone, N., Birgel, D., & Peckmann, J. (2009). Genesis of phosphorite crusts off Peru. *Marine Geology*, *262*(1), 68-81. https://doi.org/10.1016/j.margeo.2009.03.006

Atudorei, V., & Baud, A. (1997). Carbon isotope events during the Triassic. *Albertiana*, *20*, 45-49.

Bäckström, S., & Nagy, J. (1985). Depositional history and fauna of a Jurassic phosphorite conglomerate (the Brentskardhaugen Bed) in Spitsbergen.

Bergan, M., & Knarud, R. (1993). Apparent changes in clastic mineralogy of the Triassic–Jurassic succession, Norwegian Barents Sea: possible implications for palaeodrainage and subsidence. In T. O. Vorren, E. Bergsager, Ø. A. Dahl-Stamnes, E. Holter, B. Johansen, E. Lie, & T. B. Lund (Eds.), *Norwegian Petroleum Society Special Publications* (Vol. 2, pp. 481-493). Elsevier. https://doi.org/10.1016/B978-0-444-88943-0.50034-4

Bjærke, T., & Dypvik, H. (1977). Sedimentological and palynological studies of Upper Triassic-Lower Jurassic sediments in Sassenfjorden, Spitsbergen.

Bjærke, T., & Manum, S. B. (1977). Mesozoic palynology of Svalbard. I, The Rhaetian of Hopen, with a preliminary report on the Rhaetian and Jurassic of Kong Karls Land.

Blackburn, T. J., Olsen, P. E., Bowring, S. A., McLean, N. M., Kent, D. V., Puffer, J., McHone, G., Rasbury, E. T., & Et-Touhami, M. (2013). Zircon U-Pb Geochronology Links the End-Triassic Extinction with the Central Atlantic Magmatic Province. *Science*, *340*(6135), 941-945. https://doi.org/10.1126/science.1234204

Böhm, F., & Gawlick, H. J. (1997). Late Triassic carbon isotope excursion in pelagic limestones of the Northern Calcareous Alps (Abstract 18th Regional European Meeting of Sedimentology).

Bonis, N. R., Kürschner, W. M., & Krystyn, L. (2009). A detailed palynological study of the Triassic–Jurassic transition in key sections of the Eiberg Basin (Northern Calcareous Alps, Austria). *Review of Palaeobotany and Palynology*, *156*(3), 376-400. https://doi.org/10.1016/j.revpalbo.2009.04.003

Bos, R., Lindström, S., van Konijnenburg-van Cittert, J., Hilgen, F., Hollaar, T., Aalpoel, H., van der Weijst, C., Sanei, H., Rudra, A., Sluijs, A., & van de Schootbrugge, B. (2023). Triassic-Jurassic Vegetation Response to Carbon Cycle Perturbations and Climate Change. *SSRN Electronic Journal*. https://doi.org/10.2139/ssrn.4371814

Bue, E. P., & Andresen, A. (2013). Constraining depositional models in the Barents Sea region using detrital zircon U–Pb data from Mesozoic sediments in Svalbard. *Geological Society, London, Special Publications*, *386*(1), 261-279. https://doi.org/10.1144/SP386.14

Buiter, S. J. H., & Torsvik, T. H. (2007). Horizontal movements in the eastern Barents Sea constrained by numerical models and plate reconstructions. *Geophysical Journal International*, *171*(3), 1376-1389. https://doi.org/10.1111/j.1365-246X.2007.03595.x

Bujak, J. P., & Fisher, M. J. (1976). Dinoflagellate Cysts from the Upper Triassic of Arctic Canada. *Micropaleontology*, *22*(1), 44-70. https://doi.org/10.2307/1485320

Clement, A. M., Tackett, L. S., & Marolt, S. (2024). Biosediment assemblages reveal disrupted silica cycling and redox conditions throughout the Rhaetian Stage: Evidence for a precursor event to the end-Triassic mass extinction. *Palaeogeography, Palaeoclimatology, Palaeoecology*, *638*, 112034. https://doi.org/10.1016/j.palaeo.2024.112034

Crosby, C. H., & Bailey, J. V. (2012). The role of microbes in the formation of modern and ancient phosphatic mineral deposits. *Frontiers in Microbiology*, *3*. https://doi.org/10.3389/fmicb.2012.00241

Dal Corso, J., Gianolla, P., Rigo, M., Franceschi, M., Roghi, G., Mietto, P., Manfrin, S., Raucsik, B., Budai, T., Jenkyns, H. C., Reymond, C. E., Caggiati, M., Gattolin, G., Breda, A., Merico, A., & Preto, N. (2018). Multiple negative carbon-isotope excursions during the Carnian Pluvial

Episode (Late Triassic). *Earth-Science Reviews*, *185*, 732-750. https://doi.org/10.1016/j.earscirev.2018.07.004

Dal Corso, J., Marzoli, A., Tateo, F., Jenkyns, H., Bertrand, H., Youbi, N., Mahmoudi, A., Font, E., Buratti, N., & Cirilli, S. (2014). The dawn of CAMP volcanism and its bearing on the end-Triassic carbon cycle disruption. *Journal of the Geological Society*, *171*, 153-164. https://doi.org/10.1144/jgs2013-063

Dal Corso, J., Mietto, P., Newton, R. J., Pancost, R. D., Preto, N., Roghi, G., & Wignall, P. B. (2012). Discovery of a major negative 13C spike in the Carnian (Late Triassic) linked to the eruption of Wrangellia flood basalts. *Geology*, *40*(1), 79-82. https://doi.org/10.1130/g32473.1

Davies, J. H. F. L., Marzoli, A., Bertrand, H., Youbi, N., Ernesto, M., & Schaltegger, U. (2017). End-Triassic mass extinction started by intrusive CAMP activity. *Nature Communications*, *8*(1). https://doi.org/10.1038/ncomms15596

De Jersey, N. J. (1971). *Early Jurassic miospores from the Helidon Sandstone*. Queensland Geological Survey.

Dimakis, P., Braathen, B. I., Faleide, J. I., Elverhøi, A., & Gudlaugsson, S. T. (1998). Cenozoic erosion and the preglacial uplift of the Svalbard–Barents Sea region. *Tectonophysics*, *300*(1), 311-327. https://doi.org/10.1016/S0040-1951(98)00245-5

Dypvik, H., Hvoslef, S., Bjærke, T., & Finnerud, E. (1985). The Wilhelmøya Formation (Upper Triassic-Lower Jurassic) at Bohemanflya, Spitsbergen. *Polar Research*, *3*(2), 155-165. https://doi.org/10.3402/polar.v3i2.6949

Embry, A. F., & Suneby, L. B. (1994). The Triassic-Jurassic boundary in the Sverdrup Basin, Arctic Canada.

Ernst, R., & Buchan, K. (2001). Large mafic magmatic events through time and links to mantle-plume heads. In (Vol. 352, pp. 483-575). https://doi.org/10.1130/0-8137-2352-3.483

Faleide, J. I., Bjørlykke, K., & Gabrielsen, R. H. (2015). Geology of the Norwegian Continental Shelf. In *Petroleum Geoscience: From Sedimentary Environments to Rock Physics, Second Edition* (pp. 603-637). Springer Berlin Heidelberg. https://doi.org/10.1007/978-3-642-34132-8_25

Faleide, J. I., Vågnes, E., & Gudlaugsson, S. T. (1993). Late Mesozoic-Cenozoic evolution of the south-western Barents Sea in a regional rift-shear tectonic setting. *Marine and Petroleum Geology*, *10*(3), 186-214. https://doi.org/10.1016/0264-8172(93)90104-Z

Fisher, M. (1979). The Triassic palynofloral succession in the Canadian Arctic archipelago. *American Association of Stratigraphic Palynologists Contribution Series 5B*, 83-100.

Fisher, M., & Dunay, R. (1981). Palynology and the Triassic/Jurassic boundary. *Review of Palaeobotany and Palynology*, *34*(1), 129-135.

Fisher, M. J., & van Helden, B. G. T. (1979). Some observations on the fossil dinocyst genus Rhaetogonyaulax Sarjeant, 1966. *Palynology*, *3*(1), 265-276. https://doi.org/10.1080/01916122.1979.9989194

Fleming, E. J., Flowerdew, M. J., Smyth, H. R., Scott, R. A., Morton, A. C., Omma, J. E., Frei, D., & Whitehouse, M. J. (2016). Provenance of Triassic sandstones on the southwest Barents Shelf and the implication for sediment dispersal patterns in northwest Pangaea. *Marine and Petroleum Geology*, *78*, 516-535. https://doi.org/10.1016/j.marpetgeo.2016.10.005

Frebold, H. J. C. (1930). *Das Festungsprofil auf Spitzbergen*. https://books.google.nl/books?id=AmUozwEACAAJ

Frederiksen, N. O. (1980). Significance of monosulcate pollen abundance in Mesozoic sediments. *Lethaia*, *13*(1), 1-20. https://doi.org/10.1111/j.1502-3931.1980.tb01023.x

Grasby, S. E., Beauchamp, B., Bond, D. P. G., Wignall, P. B., & Sanei, H. (2016). Mercury anomalies associated with three extinction events (Capitanian Crisis, Latest Permian Extinction and the Smithian/Spathian Extinction) in NW Pangea. *Geological Magazine*, *153*(2), 285-297. https://doi.org/10.1017/s0016756815000436

Gravendyck, J., Coiffard, C., B. Bachelier, J., & Kürschner, W. (2023). Re-evaluation of Cerebropollenites thiergartii Eberh.Schulz 1967 and related taxa: priority of

Sciadopityspollenites and nomenclatural novelties. *Grana*, *62*(1), 1-47. https://doi.org/10.1080/00173134.2022.2158688

Hallam, A., & Wignall, P. B. (1999). Mass extinctions and sea-level changes. *Earth-Science Reviews*, *48*(4), 217-250. https://doi.org/10.1016/S0012-8252(99)00055-0

Hesselbo, S. P., Robinson, S. A., Surlyk, F., & Piasecki, S. (2002). Terrestrial and marine extinction at the Triassic-Jurassic boundary synchronized with major carbon-cycle perturbation: A link to initiation of massive volcanism? *Geology*, *30*(3), 251-254. https://doi.org/10.1130/0091-7613(2002)030<0251:TAMEAT>2.0.CO;2

Hiatt, E. E., Pufahl, P. K., & Edwards, C. T. (2015). Sedimentary phosphate and associated fossil bacteria in a Paleoproterozoic tidal flat in the 1.85Ga Michigamme Formation, Michigan, USA. *Sedimentary Geology*, *319*, 24-39. https://doi.org/10.1016/j.sedgeo.2015.01.006

Hochuli, P. A., & Vigran, J. O. (2010). Climate variations in the Boreal Triassic — Inferred from palynological records from the Barents Sea. *Palaeogeography, Palaeoclimatology, Palaeoecology*, *290*(1), 20-42. https://doi.org/10.1016/j.palaeo.2009.08.013

Hoel, A., & Orvin, A. K. (1937). *Das Festungsprofil auf Spitzbergen, Karbon--Kreide. I, Vermessungsresultate*. I kommisjon hos J. Dybwad.

Høy, T., & Lundschien, B. A. (2011). Triassic deltaic sequences in the northern Barents Sea. In *Arctic Petroleum Geology, Geological Society of London Memoirs* (Vol. 35, pp. 249-260). https://doi.org/10.1144/M35.15

Jin, X., Tomimatsu, Y., Yin, R., Onoue, T., Franceschi, M., Grasby, S. E., Du, Y., & Rigo, M. (2023). Climax in Wrangellia LIP activity coincident with major Middle Carnian (Late Triassic) climate and biotic changes: Mercury isotope evidence from the Panthalassa pelagic domain. *Earth and Planetary Science Letters*, *607*, 118075. https://doi.org/10.1016/j.epsl.2023.118075

Johannessen, E. P., & Embry, A. F. (1989, 1989//). Sequence correlation: Upper Triassic to Lower Jurassic succession, Canadian and Norwegian Arctic. Correlation in Hydrocarbon Exploration, Dordrecht.

Klausen, T. G., Ryseth, A. E., Helland-Hansen, W., Gawthorpe, R., & Laursen, I. (2015). Regional development and sequence stratigraphy of the Middle to Late Triassic Snadd Formation, Norwegian Barents Sea. *Marine and Petroleum Geology*, *62*, 102-122. https://doi.org/10.1016/j.marpetgeo.2015.02.004

Koevoets, M., Hammer, O., Olaussen, S., Senger, K., & Smelror, M. (2018). Integrating subsurface and outcrop data of the Middle Jurassic to Lower Cretaceous Agardhfjellet Formation in central Spitsbergen. *Norwegian Journal of Geology*, *98*. https://doi.org/10.17850/njg98-4-01

Korčinskaja, M. (1980). Rannenorijskaja fauna arhipelaga Sval'bard [Early Norian fauna of the archipelago of Svalbard]. *Geologija osadočnogo čehla arhipelaga Sval'bard (Geology of the sedimentary platform of the Archipelago of Svalbard), NIIGA, Leningrad*, 30-43.

Kürschner, W., Bonis, N. R., & Krystyn, L. (2007). Carbon-isotope stratigraphy and palynostratigraphy of the Triassic-Jurassic transition in the Tiefengraben section - Northern Calcareous Alps (Austria). *Palaeogeography Palaeoclimatology Palaeoecology*, *244*, 257-280. https://doi.org/10.1016/j.palaeo.2006.06.031

Larina, E., Bottjer, D. J., Corsetti, F. A., Zonneveld, J.-P., Celestian, A. J., & Bailey, J. V. (2019). Uppermost Triassic phosphorites from Williston Lake, Canada: link to fluctuating euxinic-anoxic conditions in northeastern Panthalassa before the end-Triassic mass extinction. *Scientific Reports*, *9*(1), 18790. https://doi.org/10.1038/s41598-019-55162-2

Lindström, S. (2016). Palynofloral patterns of terrestrial ecosystem change during the end-Triassic event - A review [Review]. *Geological Magazine*, *153*(2), 223-251. https://doi.org/10.1017/S0016756815000552

Lindström, S. (2020). *Palynology of the Gassum and lowermost Fjerritslev formations in the Stenlille area: biostratigraphic and palaeoenvironmental implications (Part of Work package 5 in the CCUS project)*.

Lindström, S. (2021). Two-phased mass rarity and extinction in land plants during the end-Triassic climate crisis. *Frontiers in Earth Science*, *9*, 780343.

Lindström, S., Callegaro, S., Davies, J., Tegner, C., van de Schootbrugge, B., Pedersen, G. K., Youbi, N., Sanei, H., & Marzoli, A. (2021). Tracing volcanic emissions from the Central Atlantic Magmatic Province in the sedimentary record. *Earth-Science Reviews*, *212*, 103444. https://doi.org/10.1016/j.earscirev.2020.103444

Lindström, S., Erlström, M., Piasecki, S., Nielsen, L. H., & Mathiesen, A. (2017). Palynology and terrestrial ecosystem change of the Middle Triassic to lowermost Jurassic succession of the eastern Danish Basin. *Review of Palaeobotany and Palynology*, *244*, 65-95. https://doi.org/10.1016/j.revpalbo.2017.04.007

Lindström, S., Pedersen, G. K., Vosgerau, H., Hovikoski, J., Dybkjær, K., & Nielsen, L. H. (2023). Palynology of the Triassic–Jurassic transition of the Danish Basin (Denmark): a palynostratigraphic zonation of the Gassum–lower Fjerritslev formations. *Palynology*, *47*(4), 2241068. https://doi.org/10.1080/01916122.2023.2241068

Lindström, S., van de Schootbrugge, B., Hansen, K. H., Pedersen, G. K., Alsen, P., Thibault, N., Dybkjær, K., Bjerrum, C. J., & Nielsen, L. H. (2017). A new correlation of Triassic–Jurassic boundary successions in NW Europe, Nevada and Peru, and the Central Atlantic Magmatic Province: A time-line for the end-Triassic mass extinction. *Palaeogeography, Palaeoclimatology, Palaeoecology*, *478*, 80-102. https://doi.org/10.1016/j.palaeo.2016.12.025

Lord, G., Johansen, S., Støen, S., & Mørk, A. (2017). Facies development of the Upper Triassic succession on Barentsøya, Wilhelmøya and NE Spitsbergen, Svalbard. *Norwegian Journal of Geology*, *97*. https://doi.org/10.17850/njg97-1-03

Lord, G. S., Solvi, K. H., Ask, M., Mork, A., Hounslow, M. W., & Paterson, N. W. (2014). The hopen member: a new member of the Triassic De Geerdalen Formation, Svalbard. *NORWEGIAN PETROLEUM DIRECTORATE BULLETIN, NO 11*, *11*, 81-96.

Loutit, T. S., Hardenbol, J., Vail, P. R., Baum, G. R., Wilgus, C. K., Hastings, B. S., Posamentier, H., Wagoner, J. V., Ross, C. A., & Kendall, C. G. S. C. (1988). Condensed Sections: The Key to Age Determination and Correlation of Continental Margin Sequences. In *Sea-Level Changes: An Integrated Approach* (Vol. 42, pp. 0). SEPM Society for Sedimentary Geology. https://doi.org/10.2110/pec.88.01.0183

Lund, J. J. (1977). Rhaetic to Lower Liassic palynology of the onshore south-eastern North Sea Basin. *Danmarks Geologiske Undersøgelse II. Række*, *109*, 1-128. https://doi.org/10.34194/raekke2.v109.6900

Mädler, K. (1964). Die geologische Verbreitung von Sporen und Pollen-in der deutschen Trias.

Mander, L., Kürschner, W. M., & McElwain, J. C. (2010). An explanation for conflicting records of Triassic–Jurassic plant diversity. *Proceedings of the National Academy of Sciences*, *107*(35), 15351-15356. https://doi.org/10.1073/pnas.1004207107

Mander, L., Kürschner, W. M., & McElwain, J. C. (2013). Palynostratigraphy and vegetation history of the Triassic–Jurassic transition in East Greenland. *Journal of the Geological Society*, *170*(1), 37-46. https://doi.org/10.1144/jgs2012-018

McGhee, G. R., Clapham, M. E., Sheehan, P. M., Bottjer, D. J., & Droser, M. L. (2013). A new ecological-severity ranking of major Phanerozoic biodiversity crises. *Palaeogeography, Palaeoclimatology, Palaeoecology*, *370*, 260-270. https://doi.org/10.1016/j.palaeo.2012.12.019

Morbey, S. (1978). Late Triassic and Early Jurassic subsurface palynostratigraphy in northwestern Europe. *Palinologia*, *1*(special issue), 355-368.

Mørk, A., Dallmann, W. K., Dypvik, H., Johannessen, E. P., Larssen, G. B., Nagy, J., Nøttvedt, A., Olaussen, S., Pčelina, T. M., & Worsley, D. (1999). Mesozoic Lithostratigraphy. In *Lithostratigraphic Lexicon of Svalbard: Review and Recommendations for Nomenclature use* (pp. pp. 127–214.). Norsk Polarinstitutt.

Nagy, J., & Berge, S. H. (2008). Micropalaeontological evidence of brackish water conditions during deposition of the Knorringfjellet Formation, Late Triassic–Early Jurassic, Spitsbergen. *Polar Research*, *27*(3), 413-427. https://doi.org/10.1111/j.1751-8369.2007.00038.x

Paterson, N. W., & Mangerud, G. (2015). Late Triassic (Carnian– Rhaetian) palynology of Hopen, Svalbard. *Review of Palaeobotany and Palynology*, *220*, 98-119. https://doi.org/10.1016/j.revpalbo.2015.05.001

Paterson, N. W., & Mangerud, G. (2017). Palynology and depositional environments of the Middle – Late Triassic (Anisian – Rhaetian) Kobbe, Snadd and Fruholmen formations, southern Barents Sea, Arctic Norway. *Marine and Petroleum Geology*, *86*, 304-324. https://doi.org/10.1016/j.marpetgeo.2017.05.033

Paterson, N. W., & Mangerud, G. (2020). A revised palynozonation for the Middle–Upper Triassic (Anisian–Rhaetian) Series of the Norwegian Arctic. *Geological Magazine*, *157*(10), 1568-1592. https://doi.org/10.1017/s0016756819000906

Paterson, N. W., Mangerud, G., Holen, L. H., Landa, J., Lundschien, B. A., & Eide, F. (2019). Late Triassic (early Carnian–Norian) palynology of the Sentralbanken High, Norwegian Barents Sea. *Palynology*, *43*(1), 53-75. https://doi.org/10.1080/01916122.2017.1413018

Pedersen, K. R., & Lund, J. J. (1980). Palynology of the plant-bearing rhaetian to hettangian kap stewart formation, scoresby sund, east greenland. *Review of Palaeobotany and Palynology*, *31*, 1-69. https://doi.org/10.1016/0034-6667(80)90022-6

Posarnentier, H. W., & Allen, G. P. (1999). *Siliciclastic Sequence Stratigraphy—Concepts and Applications*. SEPM Society for Sedimentary Geology. https://doi.org/10.2110/csp.99.07

Prokoph, A., El Bilali, H., & Ernst, R. (2013). Periodicities in the emplacement of large igneous provinces through the Phanerozoic: Relations to ocean chemistry and marine biodiversity evolution. *Geoscience Frontiers*, *4*(3), 263-276. https://doi.org/10.1016/j.gsf.2012.08.001

Pufahl, P., & Grimm, K. (2003). Coated phosphate grains: Proxy for physical, chemical, and ecological changes in seawater. *Geology*, *31*, 801-804. https://doi.org/10.1130/G19658.1

Retallack, G. (1975). The life and times of a Triassic lycopod. *Alcheringa: An Australasian Journal of Palaeontology*, *1*(1), 3-29. https://doi.org/10.1080/03115517508619477

Rigo, M., Onoue, T., Tanner, L. H., Lucas, S. G., Godfrey, L., Katz, M. E., Zaffani, M., Grice, K., Cesar, J., Yamashita, D., Maron, M., Tackett, L. S., Campbell, H., Tateo, F., Concheri, G., Agnini, C., Chiari, M., & Bertinelli, A. (2020). The Late Triassic Extinction at the Norian/Rhaetian boundary: Biotic evidence and geochemical signature. *Earth-Science Reviews*, *204*, 103180. https://doi.org/10.1016/j.earscirev.2020.103180

Riis, F., Lundschien, B., Høy, T., Mørk, A., & Mørk, M. B. (2008). Evolution of the Triassic shelf in the northern Barents Sea region. *Polar Research*, *27*, 318-338. https://doi.org/10.1111/j.1751-8369.2008.00086.x

Rismyhr, B., Bjærke, T., Olaussen, S., Mulrooney, M. J., & Senger, K. (2018). Facies, palynostratigraphy and sequence stratigraphy of the Wilhelmøya Subgroup (Upper Triassic–Middle Jurassic) in western central Spitsbergen, Svalbard. *Norwegian Journal of Geology*. https://doi.org/10.17850/njg001

Rød, R. S., Hynne, I. B., & Mørk, A. (2014). Depositional environment of the Upper Triassic De Geerdalen Formation – An E-W transect from Edgeøya to Central Spitsbergen, Svalbard. *Norwegian Petroleum Directorate Bulletin*(11), 21-40.

Ruhl, M., Bonis, N. R., Reichart, G.-J., Damsté, J. S. S., & Kürschner, W. M. (2011). Atmospheric Carbon Injection Linked to End-Triassic Mass Extinction. *Science*, *333*(6041), 430-434. https://doi.org/10.1126/science.1204255

Ruhl, M., & Kürschner, W. (2011). Multiple phases of carbon cycle disturbance from large igneous province formation at the Triassic-Jurassic transition. *Geology*, *39*(5), 431-434.

Ryseth, A. L. F. (2014). Sedimentation at the Jurassic-Triassic boundary, south-west Barents Sea: Indication of climate change. In *From Depositional Systems to Sedimentary Successions on*

the Norwegian Continental Margin (pp. 187-214). https://doi.org/10.1002/9781118920435.ch9

Sato, H., Nozaki, T., Onoue, T., Ishikawa, A., Soda, K., Yasukawa, K., Kimura, J.-I., Chang, Q., Kato, Y., & Rigo, M. (2023). Rhenium-osmium isotope evidence for the onset of volcanism in the central Panthalassa Ocean during the Norian "chaotic carbon episode". *Global and Planetary Change*, *229*, 104239. https://doi.org/10.1016/j.gloplacha.2023.104239

Simms, M. J., & Ruffell, A. H. (1989). Synchroneity of climatic change and extinctions in the Late Triassic. *Geology*, *17*(3), 265-268.

Smelror, M., Larssen, G. B., Olaussen, S., Rømuld, A., & Williams, R. (2019). Late Triassic to Early Cretaceous palynostratigraphy of Kong Karls Land, Svalbard, Arctic Norway; with correlation to Franz Josef Land, Arctic Russia. *Norwegian Journal of Geology*, 4. https://doi.org/10.17850/njg004

Smith, D. G. (1975). The stratigraphy of Wilhelmøya and Hellwaldfjellet, Svalbard. *Geological Magazine*, *112*(5), 481-491.

Smith, D. G. (1982). Stratigraphic significance of a palynoflora from ammonoid-bearing Early Norian strata in Svalbard. *Newsletters on Stratigraphy*, *11*(3), 154-161.

Smith, D. G., Harland, W. B., & Hughes, N. F. (1975). Geology of Hopen, Svalbard. *Geological Magazine*, *112*(1), 1-23. https://doi.org/10.1017/S0016756800045544

Steel, R., Gjelberg, J., Helland-Hansen, W., Kleinspehn, K., Nøttvedt, A., & Rye-Larsen, M. (1985). The Tertiary Strike-Slip Basins and Orogenic Belt of Spitsbergen. In K. T. Biddle & N. Christie-Blick (Eds.), *Strike-Slip Deformation, Basin Formation, and Sedimentation* (Vol. 37, pp. 0). SEPM Society for Sedimentary Geology. https://doi.org/10.2110/pec.85.37.0319

Suan, G., Föllmi, K., Adatte, T., Bomou, B., Spangenberg, J., & van de Schootbrugge, B. (2012). Major environmental change and bonebed genesis prior to the Triassic–Jurassic mass extinction. *Journal of the Geological Society*, *169*, 191-200. https://doi.org/10.1144/0016-76492011-045

Sun, Y. D., Orchard, M. J., Kocsis, Á. T., & Joachimski, M. M. (2020). Carnian–Norian (Late Triassic) climate change: Evidence from conodont oxygen isotope thermometry with implications for reef development and Wrangellian tectonics. *Earth and Planetary Science Letters*, *534*, 116082. https://doi.org/10.1016/j.epsl.2020.116082

Suneby, L., & Hills, L. (1988). Palynological zonation of the Heiberg Formation (Triassic-Jurassic) eastern Sverdrup Basin, Arctic Canada. *Bulletin of Canadian Petroleum Geology*, *36*(4), 347-361.

Trotter, J. A., Williams, I. S., Nicora, A., Mazza, M., & Rigo, M. (2015). Long-term cycles of Triassic climate change: a new δ18O record from conodont apatite. *Earth and Planetary Science Letters*, *415*, 165-174. https://doi.org/10.1016/j.epsl.2015.01.038

Vakhrameev, V. A. (1981). Pollen Classopolis: Indicator of Jurassic and Cretaceous climates. *Journal of Palaeosciences*, *28*, 301-307. https://doi.org/10.54991/jop.1981.1417

Van de Schootbrugge, B., Bachan, A., Suan, G., Richoz, S., & Payne, J. L. (2013). Microbes, mud and methane: cause and consequence of recurrent Early Jurassic anoxia following the end-Triassic mass extinction. *Palaeontology*, *56*(4), 685-709. https://doi.org/10.1111/pala.12034

Van de Schootbrugge, B., Quan, T. M., Lindström, S., Püttmann, W., Heunisch, C., Pross, J., Fiebig, J., Petschick, R., Röhling, H. G., Richoz, S., Rosenthal, Y., & Falkowski, P. G. (2009). Floral changes across the Triassic/Jurassic boundary linked to flood basalt volcanism. *Nature Geoscience*, *2*(8), 589-594. https://doi.org/10.1038/ngeo577

van de Schootbrugge, B., Tremolada, F., Rosenthal, Y., Bailey, T. R., Feist-Burkhardt, S., Brinkhuis, H., Pross, J., Kent, D. V., & Falkowski, P. G. (2007). End-Triassic calcification crisis and blooms of organic-walled 'disaster species'. *Palaeogeography, Palaeoclimatology, Palaeoecology*, *244*(1), 126-141. https://doi.org/10.1016/j.palaeo.2006.06.026

Vigran, J., Mangerud, G., Mørk, A., Worsley, D., & Hochuli, P. (2014). Palynology and geology of the Triassic succession of Svalbard and the Barents Sea. *Geological Survey of Norway*, *Special Publication*, 275 pp. https://doi.org/10.5167/uzh-99116

von Hillebrandt, A., Krystyn, L., & Kürschner, W. (2007). A candidate GSSP for the base of the Jurassic in the Northern Calcareous Alps (Kuhjoch section, Karwendel Mountains, Tyrol, Autria). *International Subcommission on Jurassic Stratigraphy Newsletter*, *34*.

von Hillebrandt, A., Krystyn, L., Kürschner, W. M., Bonis, N. R., Ruhl, M., Richoz, S., Schobben, M. A. N., Urlichs, M., Bown, P. R., Kment, K., McRoberts, C. A., Simms, M., & Tomãsových, A. (2013). The Global Stratotype Sections and Point (GSSP) for the base of the Jurassic System at Kuhjoch (Karwendel Mountains, Northern Calcareous Alps, Tyrol, Austria). *Episodes*, *36*(3), 162-198. https://doi.org/10.18814/epiiugs/2013/v36i3/001

Ward, P. D., Garrison, G. H., Haggart, J. W., Kring, D. A., & Beattie, M. J. (2004). Isotopic evidence bearing on Late Triassic extinction events, Queen Charlotte Islands, British Columbia, and implications for the duration and cause of the Triassic/Jurassic mass extinction. *Earth and Planetary Science Letters*, *224*(3), 589-600. https://doi.org/10.1016/j.epsl.2004.04.034

Whiteside, J. H., Olsen, P. E., Eglinton, T., Brookfield, M. E., & Sambrotto, R. N. (2010). Compound-specific carbon isotopes from Earth's largest flood basalt eruptions directly linked to the end-Triassic mass extinction. *Proceedings of the National Academy of Sciences*, *107*(15), 6721-6725. https://doi.org/10.1073/pnas.1001706107

Wignall, P. B. (2001). Large igneous provinces and mass extinctions. *Earth-Science Reviews*, *53*(1), 1-33. https://doi.org/10.1016/S0012-8252(00)00037-4

Wignall, P. B., & Atkinson, J. W. (2020). A two-phase end-Triassic mass extinction. *Earth-Science Reviews*, *208*, 103282. https://doi.org/10.1016/j.earscirev.2020.103282

Williford, K., Orchard, M., Zonneveld, J.-P., McRoberts, C., & Beatty, T. W. (2007). A record of stable organic carbon isotopes from the Carnian-Norian boundary section at Black Bear Ridge, Williston Lake, British Columbia, Canada. *Albertiana*, *36*, 146-148.

Winsnes, T. S., Heintz, A., & Heintz, N. (1962). Aspects of the geology of Svalbard.

Worsley, D. (2008). The post-Caledonian development of Svalbard and the western Barents Sea. *27*(3). https://doi.org/10.3402/polar.v27i3.6197

Zaffani, M., Agnini, C., Concheri, G., Godfrey, L., Katz, M., Maron, M., & Rigo, M. (2017). The Norian "chaotic carbon interval": new clues from the δ13Corg record of the Lagonegro Basin (southern Italy). *Geosphere*, *13*(4), 1133-1148.

Zaffani, M., Jadoul, F., & Rigo, M. (2018). A new Rhaetian δ13Corg record: Carbon cycle disturbances, volcanism, End-Triassic mass Extinction (ETE). *Earth-Science Reviews*, *178*, 92-104. https://doi.org/10.1016/j.earscirev.2018.01.004

Appendices

Appendix 1: Counting of phosphatic grains

The amount of phosphatic grains counted per sample. Grains were quantified by counting through the long side of the thin sections 3 times at 10x magnification. The three samples containing phosphatic coated grains are marked by a coated grain icon. On the right: a picture of the monomictic phosphorite conglomerate at the base of the Slottet Bed at the Festningen outcrop is shown (Rismyhr et al., 2018).

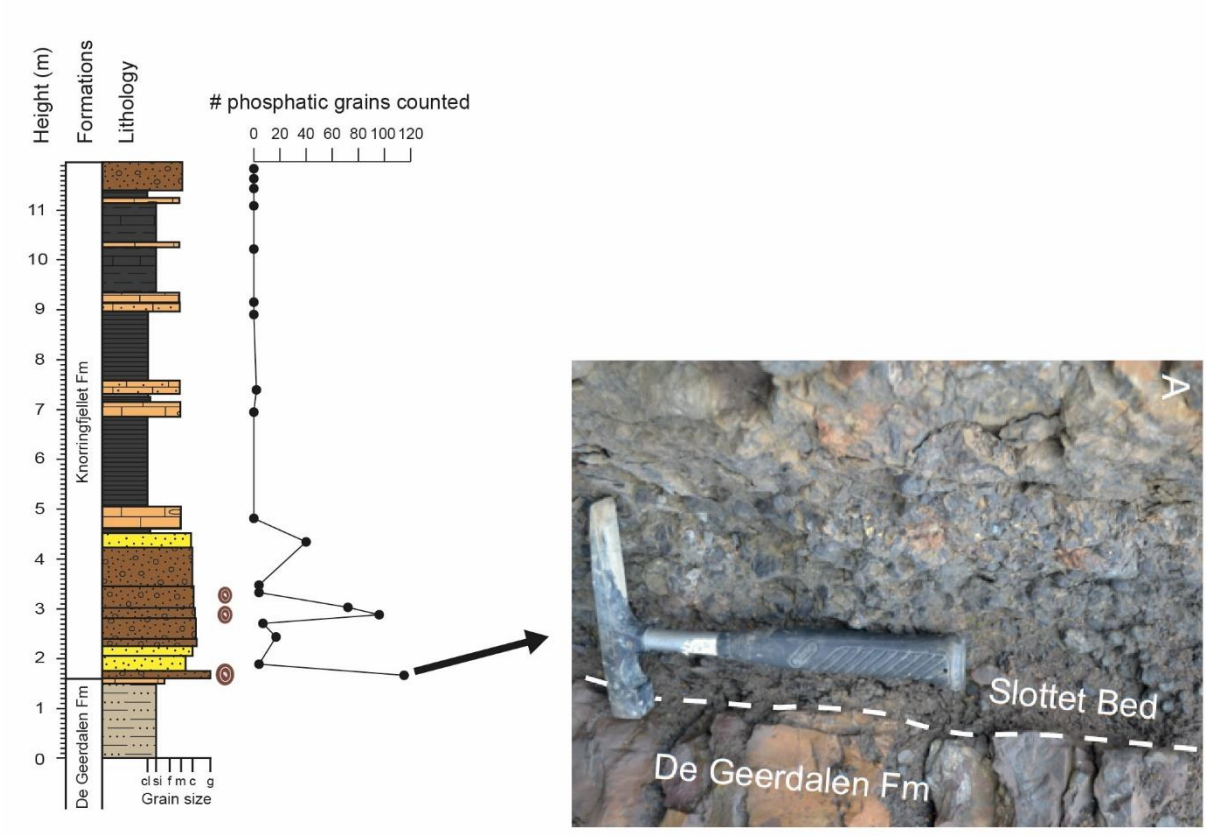

Appendix 2: Palynological range chart with all clearly present taxa